

Crossover between BCS Superconductor and Doped Mott Insulator of d -wave Pairing State in Two-Dimensional Hubbard Model

Hisatoshi YOKOYAMA^{1*}, Masao OGATA², Yukio TANAKA³, Kenji KOBAYASHI⁴,
and Hiroki TSUCHIURA⁵

¹*Department of Physics, Tohoku University, Sendai 980-8578, Japan*

²*Department of Physics, University of Tokyo, Bunkyo-ku, Tokyo 113-0033, Japan*

³*Department of Applied Physics, Nagoya University, Nagoya 464-8603, Japan*

⁴*Department of Natural Science, Chiba Institute of Technology, Narashino 275-0023, Japan*

⁵*Department of Applied Physics, Tohoku University, Sendai 980-8579 Japan*

With high- T_c cuprates in mind, the properties of correlated $d_{x^2-y^2}$ -wave superconducting (SC) and antiferromagnetic (AF) states are studied for the Hubbard (t - t' - U) model on square lattices using a variational Monte Carlo method. We employ simple trial wave functions including only crucial parameters, such as a doublon-holon binding factor indispensable for describing correlated SC and normal states as doped Mott insulators. The U/t , t'/t , and δ (doping rate) dependences of relevant quantities are systematically calculated. As U/t increases, a sharp crossover of SC properties occurs at $U_{co}/t \sim 10$ from a conventional BCS type to a kinetic-energy-driven type for any t'/t . As δ decreases, U_{co}/t is smoothly connected to the Mott transition point at half filling. For $U/t \lesssim 5$, steady superconductivity corresponding to the cuprates is not found, whereas the d -wave SC correlation function P_d^∞ rapidly increases for $U/t \gtrsim 6$ and becomes maximum at $U = U_{co}$. Comparing the δ dependence of P_d^∞ with an experimentally observed dome-shaped T_c and condensation energy, we find that the effective value of U for cuprates should be larger than the bandwidth, for which the t - J model is valid. Analyzing the kinetic energy, we reveal that, for $U > U_{co}$, only doped holes (electrons) become charge carriers, which will make a small Fermi surface (hole pocket), but for $U < U_{co}$ all the electrons (holes) contribute to conduction and will make an ordinary large Fermi surface, which is contradictory to the feature of cuprates. By introducing an appropriate negative (positive) t'/t , the SC (AF) state is stabilized. In the underdoped regime, the strength of SC for $U > U_{co}$ is determined by two factors, i.e., the AF spin correlation, which creates singlet pairs (pseudogap), and the charge mobility dominated by Mott physics. In this connection, we argue that the electrons near the antinodal points in the momentum space play a leading role in stabilizing the d -wave state, in contrast to the dichotomy of electronic roles in the momentum space proposed for the two-gap problem. We also show the instability of the hole-doped AF state against phase separation.

KEYWORDS: superconductivity, cuprate, antiferromagnetism, pseudogap, doped Mott insulator, doublon-holon binding, Hubbard model, strong correlation, variational Monte Carlo method.

1. Introduction

The essence of superconductivity (SC) in high- T_c cuprates is most probably captured using two-dimensional (2D) t - J and Hubbard models;^{1,2} a variety of theories have been developed on the basis of these models.³⁻⁵ In the ground state of the t - J -type models, which deal with strongly correlated regimes, different approaches concluded that superconducting (SC) states with $d_{x^2-y^2}$ -wave symmetry are stabilized in the parameter range relevant to cuprates, as we will see further in §2.1. Meanwhile, approaches starting from the weak-correlation limit^{6,7} of the Hubbard model provided complementary, but often qualitative, views of SC for cuprates, particularly in terms of thermal and dynamical properties. Nevertheless, quantum Monte Carlo (QMC) methods,⁸⁻¹⁰ which are quantitatively reliable approaches for finite correlation strengths, unanimously yielded a result that the SC correlation function never develops in weakly correlated regimes as compared with the noninteracting case, and therefore cast serious doubt on the validity of applying weak-correlation theories to real-

istic correlation strengths. Thus, it is important to clarify how the properties of a $d_{x^2-y^2}$ -wave SC state evolve as the correlation strength is increased in the Hubbard model.

To this end, the variational Monte Carlo (VMC) method^{11,12} is useful for its continuous applicability from weakly to strongly correlated regimes in a quantitative manner. This is by virtue of the correct treatment of local electron correlations. Since the early stage of research on cuprates, VMC studies¹³⁻¹⁵ have mainly treated t - J -type models and yielded results basically consistent with the behavior of cuprates.⁵ Later, the present authors studied a many-body SC state, applying it to the 2D Hubbard (t - t' - U) model [U : onsite Coulomb correlation, t , t' : hopping integrals to the nearest-neighbor (NN) and diagonal sites].¹⁶⁻¹⁹ In refs. 16 (for $t' = 0$) and 17, we discussed superconductor (SC)-insulator (Mott) transitions at half filling arising at $U = U_c \sim 7t$ without directly introducing an antiferromagnetic (AF) correlation. According to these and recent studies,^{20,21} the binding effect between a doubly occupied site (doublon, D) and an empty site (holon, H) plays a leading role in nonmagnetic Mott transitions. Reference 16 also showed in doped cases that a

sharp crossover exists at $U = U_{\text{co}} \sim W$ [$W (= 8t)$: bandwidth], where the nature of the $d_{x^2-y^2}$ -wave SC state, Ψ_Q^d , changes qualitatively from a conventional Bardeen-Cooper-Schrieffer (BCS) type for $U < U_{\text{co}}$ to an unconventional strongly correlated type for $U > U_{\text{co}}$, in which Ψ_Q^d is stabilized by the reduction in kinetic energy. This crossover for SC is smoothly connected to the Mott transition at half filling ($U_{\text{co}} \rightarrow U_c$) as the doping rate δ is decreased. Thus, the strongly correlated SC state for $U > U_{\text{co}}$ corresponds to a doped Mott insulator,²² and is strongly affected by the effect of D-H binding correlation.

In this paper, as an extension of refs. 16 and 17, we study SC and antiferromagnetism (AF) independently for doped cases by systematically changing U/t , t'/t , and δ , using D-H binding wave functions. The primary purpose of this paper is to establish that the nature of SC is qualitatively different between the regimes of $U < U_{\text{co}}$ and $U > U_{\text{co}}$ by studying various quantities, and that the behavior of cuprates is contradictory to that of d -wave BCS-type SC realized for $U < U_{\text{co}}$ in various aspects, but consistent with the behavior of doped Mott insulators ($U > U_{\text{co}}$).

The second purpose of this study is to consider the differentiation or dichotomy of electronic roles in momentum space,^{23,24} in connection with the pseudogap problem. Early experimental studies on the so-called two-gap problem^{25–28} challenged the familiar view that the pseudogap stems from incoherent pairs of electrons^{29–32} for $T_c < T < T^*$. Two characteristic energy scales (gaps) were discovered whose δ dependences are mutually opposite in the underdoped regime. They seemed to stem from electrons with wave numbers near the nodal ($\pi/2, \pi/2$) and antinodal ($\pi, 0$) points, and correspond to the SC gap and pseudogap, respectively, indicating that the origin of the pseudogap is not directly connected to pairing. Recent experiments on the pseudogap have taken on more complicated aspects,^{33–40} and are still actively developing.^{41,42} In this study, we argue that the two energy scales can be interpreted as a pairing gap and its correction by the charge fluctuation released from a Mott insulating state, and that the electronic states near the antinodal point ($\pi, 0$) [not in the nodal region $\sim (\pi/2, \pi/2)$] are crucial to the d -wave SC.^{32,43}

Some of the results were reported previously.^{44,45}

The rest of this paper is organized as follows: In §2, we explain the model and method used in this paper. In §3, we present the results for $t' = 0$ to grasp basic features of the U/t and δ dependences of relevant quantities, and argue the existence of a crossover and its relevance to cuprates. In §4, we discuss the effects of the diagonal transfer t' , which provides a clue to understanding the stability of the SC and AF states. In §5, we argue that the electrons near the antinodal point play a leading role in realizing the d -wave SC. In §6, the main results are summarized. In Appendix A, we give supplementary explanations of the model. In Appendix B, we compare some forms of doublon-holon binding factors as a supplement to §2.2. In Appendix C, we describe in detail the definition and justification of the long-distance value of the d -wave pair correlation function in the present cases.

2. Formalism

In §2.1, we explain the Hubbard model and the background of this study. In §2.2, we introduce the many-body trial wave functions used in this paper. In §2.3, we briefly summarize the setting of VMC calculations.

2.1 Hubbard model for cuprates

As a model of the CuO_2 planes, we consider the Hubbard model on a square lattice:

$$\begin{aligned} \mathcal{H} &= \mathcal{H}_{\text{kin}} + \mathcal{H}_U \\ &= \sum_{\mathbf{k}\sigma} \varepsilon(\mathbf{k}) c_{\mathbf{k}\sigma}^\dagger c_{\mathbf{k}\sigma} + U \sum_j d_j, \end{aligned} \quad (1)$$

with $d_j = n_{j\uparrow}n_{j\downarrow}$ (doublon projector) and $n_{j\sigma} = c_{j\sigma}^\dagger c_{j\sigma}$. Although the band structure $\varepsilon(\mathbf{k})$ is qualitatively important,^{46–52} we consider, for clarity, only the minimum terms to distinguish the material dependence, i.e., NN (t) and diagonal-neighbor (t') hoppings:

$$\varepsilon(\mathbf{k}) = -2t(\cos k_x + \cos k_y) - 4t' \cos k_x \cos k_y. \quad (2)$$

We use t and the lattice constant as the units of energy and length, respectively. As discussed in Appendix A, the effective onsite repulsion U/t may differ between electron-doped and hole-doped cases. For ease of calculation, we can restrict the electron density to $n = N/N_s \leq 1$ (N : electron number; N_s : site number), or the doping rate to $\delta = 1 - n \geq 0$ by a canonical transformation. Then, t'/t becomes negative (positive) in hole- (electron-)doped cases (see Appendix A).

Studies of this model for cuprates are roughly classified into weak- and strong-correlation theories. In the former,⁶ the stability and some properties of $d_{x^2-y^2}$ -wave SC are discussed using RPA,⁵³ FLEX approximations,⁵⁴ renormalization-group,⁷ and perturbative^{55,56} approaches. As we will show in §3 and §4, however, no substantial enhancement of the SC correlation function appropriate for high- T_c cuprates is found in a weak-correlation regime ($U/t \lesssim 5$). Such a result is not restricted to our studies. Early QMC studies⁸ drew negative conclusions for the appearance of SC in the weak-coupling regime ($U/t = 2-4$). A recent QMC study⁹ using an expansion with Gaussian bases also obtained a negative result for SC in the overdoped regime up to $U/t = 7$ for $t' = 0$. Another recent study¹⁰ concluded that the $d_{x^2-y^2}$ -wave pair susceptibility is not enhanced for $t' = 0$, but an SC Kosterlitz-Thouless transition exists for moderately large values of U/t and $t'/t = -0.2$. Thus, it is improbable that the small- U/t Hubbard model with $t' = 0$ gives such a high T_c that cuprates display; a doubt arises as to the reliability of the weak-correlation theories for cuprates, at least in a quantitative sense. In this connection, we will check whether or not the introduction of the t'/t term can enhance SC in the weak-correlation regime.

In the strong-correlation limit, the Hubbard model is mapped to t - J -type models, in which robust $d_{x^2-y^2}$ -wave SC is found by the VMC,^{13–15} exact diagonalization,⁵⁷ and projector Monte Carlo methods,⁵⁸ besides by various mean-field-type approximations.^{4,5} In the corresponding

and its competition with AF orders were found near half filling by VMC studies^{59–61} using trial functions similar to ours.^{16–19} Another promising quantitative method of treating this regime is the extension of the dynamical mean field theory (DMFT). First, using a dynamical cluster approximation, a finite-temperature instability in d -wave SC was found.⁶² Subsequently, the stability of d -wave SC and the competition with AF were studied using different variations of DMFT.^{63–65} To our knowledge, there are no theories that reliably drew negative results for SC in this regime. It seems appropriate to assume that robust $d_{x^2-y^2}$ -wave SC corresponding to high- T_c cuprates is realized in the Hubbard model with $U \gtrsim W$ near half filling.

Finally, we discuss the coexistence of d -wave SC and AF long-range orders. This problem has been repeatedly addressed for the 2D t - J and Hubbard models, using, e.g., VMC methods^{59,66,67} and DMFT.^{63,68} These studies found the stability of coexisting states against both pure d -wave and AF states near half filling; other studies^{65,69,70} showed that such mixing states appear for a small δ only under certain conditions. Experimentally, no explicit evidence of microscopic coexistence has been obtained for most high- T_c cuprates,⁷¹ except for multilayered Hg systems.^{72–74} It is probable that the coexistence can be realized in clean CuO_2 planes in multilayered systems, while the absence of the coexistence in usual cases will be due to disorder. Meanwhile, inhomogeneous phases such as stripes⁷⁵ can compete or coexist with the $d_{x^2-y^2}$ wave SC.^{41,42,76} Anyway, as a basis to tackle complicated states, it is vital to study the pure d -wave and AF states separately and their competition.

2.2 Variational wave functions

We implement a series of VMC calculations. Removing irrelevant variational parameters, we elucidate basic behaviors of simple correlated d -wave SC and AF wave functions of the Jastrow type,⁷⁷

$$\Psi = \mathcal{P}\Phi, \quad (3)$$

when it is applied to the Hubbard model, eq. (1). Here, \mathcal{P} denotes a many-body correlation (Jastrow) factor composed of projection operators, and Φ a one-body (mean-field) wave function given by a Slater determinant.

In the many-body part, we consider two projection operators: $\mathcal{P} = \mathcal{P}_Q \mathcal{P}_G$.^{16,17} Although the onsite repulsive (Gutzwiller) projector⁷⁸

$$\mathcal{P}_G = \prod_j [1 - (1 - g)d_j], \quad (4)$$

with $0 \leq g \leq 1$, is of primary importance, intersite correlation factors are indispensable for a qualitatively correct description of Hubbard-type models.⁷⁹ Among them, an attractive factor between a doublon and a holon is crucial at half filling, which is defined as^{80,81}

$$\mathcal{P}_Q = \prod_j (1 - Q_j), \quad (5)$$

where $Q_j (=Q_j^S)$ is the D-H projector of site j :

$$Q_j^S = \mu \left[d_j \prod_{\tau} (1 - h_{j+\tau}) + h_j \prod_{\tau} (1 - d_{j+\tau}) \right]. \quad (6)$$

Here, $h_j = (1 - n_{j\uparrow})(1 - n_{j\downarrow})$ and τ runs over all the NN sites of site j . The projector \mathcal{P}_Q with Q_j^S yields $(1 - \mu)^{\mathcal{N}_D + \mathcal{N}_H}$ if isolated \mathcal{N}_D doublons and \mathcal{N}_H holons exist in the electron configuration, where an isolated doublon (holon) indicates a doublon (holon) not accompanied by holons (doublons) in its four NN sites. The parameter μ (≤ 1) controls the strength of the D-H correlation; for $\mu = 1$, a doublon and a holon are completely bound in mutually NN sites, for $\mu = 0$, they are completely free, and for $\mu < 0$, they become repulsive to one another. As we repeatedly showed, \mathcal{P}_Q or its analog plays a leading role in inducing conductor (metal)-to-nonmagnetic insulator (Mott) transitions^{17,20,21,82} and spin-gap transitions in attractive Hubbard models.^{83,84} Recent studies using more elaborate long-range D-H factors^{20,21} showed that the simplest NN form Q_j^S works unexpectedly well. We use the form Q_j^S for $\delta = 0$ in this study. We found that a D-H correlation factor is still important for $\delta \neq 0$ ¹⁶ if δ is roughly within the range of SC for cuprates. An NN D-H pair yields, with a single hopping process, an antiparallel-spin pair, which contributes to the pairing in d -wave SC. Because the symmetry between a doublon and a holon is broken for $\delta \neq 0$, an asymmetric form of Q_j seems reasonable. Thus, for $\delta > 0$, we use the simple asymmetric form

$$Q_j = Q_j^D = \mu d_j \prod_{\tau} (1 - h_{j+\tau}), \quad (7)$$

for ease of calculation. In Appendix B, we check different forms of Q_j in detail. The main conclusion is that the details of Q_j make no difference at least qualitatively; a simple form of Q_j such as eq. (7) preserves the essence of the D-H binding mechanism. In §3.1, we will discuss the condition that the D-H binding factor becomes significant.

In the frustrated cases ($t' \neq 0$), the D-H correlation between diagonal sites may also play a certain role. Therefore, we similarly introduce a D-H projector Q'_j with a variational parameter μ' for interdiagonal sites. Eventually, the D-H factor for $t' \neq 0$ becomes

$$\mathcal{P}_Q = \prod_j (1 - Q_j) (1 - Q'_j). \quad (8)$$

In most calculations for $t' = 0$, we fixed μ' at zero, because the optimized μ' is small and the energy gain thereof is very small ($\sim 10^{-4}t$ even for a large U/t).⁸⁵

Now, we turn to the one-body function Φ in eq. (3). As a continuation of preceding studies, we mainly study a fixed- N $d_{x^2-y^2}$ -wave singlet (BCS) state, $\Phi_d(\Delta_d, \zeta)$.⁸⁶

$$\Phi_d = \left(\sum_{\mathbf{k}} a_{\mathbf{k}} c_{\mathbf{k}\uparrow}^{\dagger} c_{-\mathbf{k}\downarrow}^{\dagger} \right)^{\frac{N}{2}} |0\rangle, \quad (9)$$

with

$$a_{\mathbf{k}} = \frac{v_{\mathbf{k}}}{\epsilon_{\mathbf{k}}} = \frac{\Delta_{\mathbf{k}}}{\sqrt{\epsilon_{\mathbf{k}}^2 + \Delta_{\mathbf{k}}^2}}, \quad (10)$$

where ζ is a variational parameter that is reduced to the chemical potential for $U/t \rightarrow 0$. Since the $d_{x^2-y^2}$ -wave is the most stable among various gap shapes near half filling,^{13,14} here we exclusively treat the basic $d_{x^2-y^2}$ -wave gap:⁸⁷⁻⁹¹

$$\Delta_{\mathbf{k}} = \Delta_d(\cos k_x - \cos k_y). \quad (11)$$

We should emphasize that, even if the variational parameter Δ_d indicates the magnitude of the d -wave singlet gap, a many-body state ($\Psi^d = \mathcal{P}\Phi_d$) with a finite Δ_d does not necessarily mean an SC state.^{92,93} To confirm the SC order, one needs to calculate the order parameter¹³ or pair correlation functions such as $P_d(\mathbf{r})$, which will be introduced later. For $\Delta_d = 0$, Φ_d is reduced to the Fermi sea Φ_F ; in this study, we use $\Psi^F (= \mathcal{P}\Phi_F)$ as the reference normal state for the energy gain by Δ_d (or Δ_{AF}). Furthermore, we fix t'/t in $\varepsilon_{\mathbf{k}}$ in the wave functions [eq. (10)] at the same value as that in the Hamiltonian, eq. (2), namely, we do not explicitly introduce a band renormalization effect due to correlation. Because the renormalization of $\varepsilon_{\mathbf{k}}$ ⁹⁴ brings about a serious effect in the vicinity of half filling,⁹⁵ we will treat this issue in upcoming publications. As n moves away from half filling, the renormalization effect rapidly becomes modest.^{51,88}

In this study, we consider a correlated AF-ordered state $\Psi_Q^{AF}(= \mathcal{P}\Phi_{AF})$ independently of the d -wave state; as a one-body state, we use a Hartree-Fock solution on the square lattice, $\Phi_{AF}(\Delta_{AF})$:⁹⁶

$$\Phi_{AF} = \prod_{\mathbf{k}} \alpha_{\mathbf{k}\uparrow}^\dagger \prod_{\mathbf{k}} \alpha_{\mathbf{k}\downarrow}^\dagger, \quad (12)$$

with

$$\alpha_{\mathbf{k}\sigma}^\dagger = u_{\mathbf{k}} c_{\mathbf{k}\sigma}^\dagger + \text{sgn}(\sigma) v_{\mathbf{k}} c_{\mathbf{k}+\mathbf{Q}\sigma}^\dagger, \quad (13)$$

where $\text{sgn}(\sigma) = 1$ or -1 according to $\sigma = \uparrow$ or \downarrow , \mathbf{Q} is the AF nesting vector (π, π) , and

$$u_{\mathbf{k}}(v_{\mathbf{k}}) = \sqrt{\frac{1}{2} \left[1 - (+) \frac{\gamma_{\mathbf{k}}}{\sqrt{\gamma_{\mathbf{k}}^2 + \Delta_{AF}^2}} \right]}, \quad (14)$$

with $\gamma_{\mathbf{k}} = -2t(\cos k_x + \cos k_y)$. In the products of eq. (12), we take \mathbf{k} -points in the Fermi sea determined by $\varepsilon_{\mathbf{k}}$ for convenience of optimization; namely, we do not allow for band renormalization, similarly to Φ_d .

2.3 Conditions of VMC calculations

In optimizing parameters, we employ a simple method that repeatedly applies one-dimensional minimization (Brent method) to every parameter⁹⁷ with the others fixed, because the number of parameters is small (≤ 6). We call the procedure in which every parameter is optimized once a ‘round’ here. In most cases, the parameters and energy converge in a few rounds of loops except in special cases near Mott transitions. To reduce the statistical error, we continue the iteration for another 15-20 rounds after the convergence, and average the data accumulated in this additional process. In each loop, we use 2.5×10^5 (typical)- 10^6 fixed samples; consequently, the results in optimization are substantially averages of several

and energy being on the order of 10^{-3} and $10^{-4}t$, respectively. In the calculations of physical quantities using the optimized parameter sets, we averaged at least 2.5×10^5 samples.

To check the system-size dependence, we use systems of $N_s = L \times L$ sites typically with $L = 10-16$, imposing the periodic(x)-antiperiodic(y) boundary conditions to reduce level degeneracy. In principle, we aim to satisfy the closed-shell condition, because open-shell systems bring about serious finite-size effects for small values of U/t , especially in the SC correlation function. However, when we treat the t'/t dependence with other parameters fixed, we are obliged to use systems with open shells in addition to those with closed shells. In this connection, as we vary t'/t , the manner of \mathbf{k} -point occupation in Φ , especially in Φ_{AF} and Φ_F , undergoes discontinuous changes at the values of t'/t specific to the system size. Consequently, a large and irregular system-size dependence on t'/t occurs in most quantities even in large- U/t cases, as we will encounter in §4. At any rate, we managed not to be affected by special cases by checking different systems.

3. Properties for $t' = 0$

We discuss the results for $t' = 0$ first to grasp the U/t and δ dependences of various quantities. In §3.1, we consider the relation of the D-H binding to the Mott physics. In §3.2, by analyzing energies, we study the crossover of the SC properties, the competition between SC and AF, and the instability of the AF state against phase separation. In §3.3, we consider the U/t dependence of correlation functions. In §3.4, we argue that, in the underdoped regime, the δ dependence is different between the quantities derived from pairing and those from charge itinerancy, and that the strength of SC is represented by their product. In §3.5, a change in the mechanism of conduction is discussed.

3.1 Relation of D-H binding to Mott physics

In Fig. 2 in ref. 16, we showed that the D-H binding correlation is highly effective for large values of U/t and small doping rates. Before discussing the main results, here we summarize this feature for $t' = 0$; the feature for finite t'/t is basically the same as that for $t' = 0$.

Figure 1 shows the optimized D-H correlation parameter μ [eqs. (6) and (7)]. Generally, as U/t increases, μ increases, namely, the D-H binding becomes tighter, for the normal and SC states. The behavior near half filling is sharply distinguished according as U is smaller than U_c (Mott critical value) or not. For $U < U_c$, μ remains small ($\mu \lesssim 0.5$) and decreases as L increases at $\delta = 0$, as indicated by an arrow, whereas for $U > U_c$, μ increases steadily as δ decreases, abruptly approaches 1 for $\delta \rightarrow 0$, and increases as L increases. Thus, μ is still relevant to the Mott physics in doped systems. In the AF state, the D-H factor is redundant, as discussed in ref. 16; this redundancy is recognized from the behavior almost independent of δ in Fig. 1.

The effect of the D-H factor is clearer in energy improvement. Figure 2(a) shows the difference in total en-

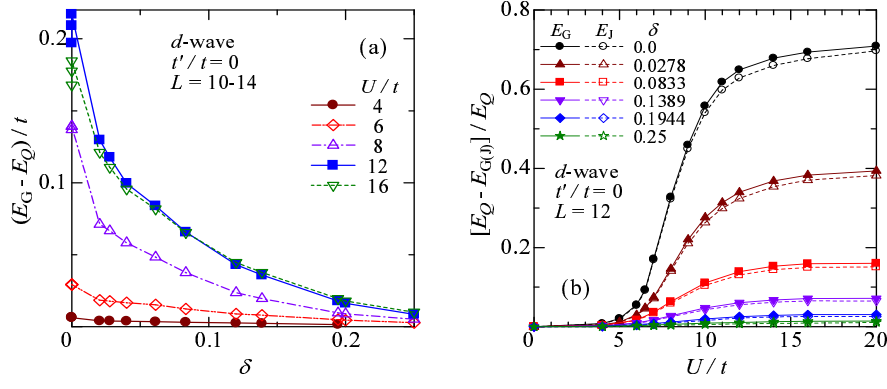


Fig. 2. (Color online) Improvement in energy by D-H binding factor on simple Gutzwiller projection in d -wave state. (a) Energy difference between Ψ_Q^d and Ψ_G^d as function of doping rate for five values of U/t . (b) Energy difference between Ψ_Q^d and Ψ_G^d normalized by E_Q as function of U/t for six doping rates. The dashed lines with open symbols indicate the values obtained using Ψ_J^d instead of Ψ_G^d .

Table I. Energy improvements by Ψ_Q^d and Ψ_J^d over E_G of Ψ_G^d in percent, i.e., $[E_{Q(J)} - E_G]/E_G \times 100$, are listed for three values of U/t and δ .

δ	$U/t \rightarrow$	4	8	12
0	Ψ_Q	0.81	48.7	184.9
	Ψ_J	0.08	0.7	5.8
0.083	Ψ_Q	0.33	17.1	16.1
	Ψ_J	0.06	0.5	0.9
0.194	Ψ_Q	0.15	2.8	2.6
	Ψ_J	0.08	0.2	0.4

$\Psi_G^d = \mathcal{P}_G \Phi_d(E_G)$. The energy gain by \mathcal{P}_Q increases as δ decreases. For $U < U_c$, however, the gain remains small even at half filling (see also Table I). This feature is evident in Fig. 2(b), where the U/t dependence is shown; the improvement is negligible for $U/t \lesssim 5$. In contrast, the energy gain becomes sizable for $U \gtrsim U_c$, where E is markedly improved by \mathcal{P}_Q at $\delta = 0$ [Fig. 2(a)]. Although the energy gain by \mathcal{P}_Q decreases as δ increases, \mathcal{P}_Q still brings appreciable improvement for $0 \leq \delta \lesssim 0.15$. This is roughly consistent with experiments on cuprates.^{98,99}

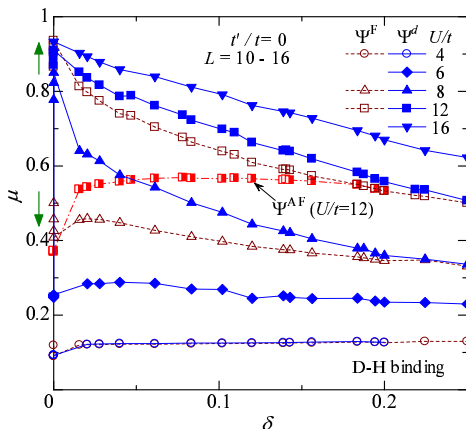


Fig. 1. (Color online) Optimized D-H binding parameters in the normal (Ψ_F^d), d -wave (Ψ_Q^d), and antiferromagnetic (Ψ_{AF}^d) states as functions of doping rate for some values of U/t . The arrows near the vertical axis indicate the directions of the system-size dependence (as L increases) at $\delta = 0$ for $U > U_c$ and $U < U_c$. The data for $L = 10-16$ are plotted together. The Mott transition points are estimated at $U_c/t \sim 7$ and 9 for Ψ_Q^d and Ψ_F^d , respectively.¹⁷

For large values of U/t , the contribution of \mathcal{P}_Q amounts to 2/3 of the total E_Q at half filling, and remains at about 7% even for $\delta \sim 0.15$.

The D-H binding correlation has a close relation to the spin exchange coupling, because an NN D-H pair yields an NN antiparallel spin pair with a single hopping. Correspondingly, the behavior of energy improvement in Figs. 2(a) and 2(b) becomes highly similar to that of the spin structure factor $S(\mathbf{q})$ at $\mathbf{q} = (\pi, \pi)$ as will be shown later in Figs. 14 and 10(a), respectively.⁴⁵ Then, the effective range of \mathcal{P}_Q in the U/t - δ space coincides with the range of robust d -wave pairing [see Δ_d as will be shown later in Figs. 11(b) and 5], because the d -wave pairing is mainly mediated by the AF spin correlation. Thus, the D-H binding correlation is crucial to the d -wave SC, and Ψ_Q^d literally represents a doped Mott insulator for $U > U_c$.

Having focused on attractive correlation as intersite factors, here we check that intersite repulsive correlation factors are irrelevant near half filling. For this purpose, we consider the typical NN repulsive Jastrow factor

$$\mathcal{P}_J = \rho_D^{\hat{N}_{DD}} \rho_H^{\hat{N}_{HH}}, \quad (15)$$

with ρ_D and ρ_H being variational parameters, and

$$\hat{N}_{DD} = \sum_{j,\tau} d_j d_{j+\tau}, \quad \hat{N}_{HH} = \sum_{j,\tau} h_j h_{j+\tau}, \quad (16)$$

where j runs over all the lattice sites, and τ NN sites of site j . We compare the improvement in energy by $\Psi_J^d = \mathcal{P}_J \mathcal{P}_G \Phi_d(E_J)$ with that of Ψ_Q^d over E_G in Table I. In every case, the energy improvement by Ψ_J^d is much smaller than that by Ψ_Q^d . In Fig. 2(b), we plot $(E_Q - E_J)/E_Q$ for comparison with the case of E_G ; the insignificance of \mathcal{P}_J is evident in the present parameter regime. Long-range Jastrow factors are also considered irrelevant for $\delta \sim 0$, by inferring from the study at half filling.^{20,21} Henceforth, we disregard intersite repulsive factors.

3.2 Energy gain by d -wave gap

Now, we consider SC properties. We begin with the energy gain (ΔE) by the d -wave gap parameter Δ_d :

$$\Delta E = E(0) - E(\Delta_d^{\text{opt}}), \quad (17)$$

where $E(\Delta_d)$ denotes the total energy for which the variational parameters other than Δ_d are optimized, and Δ_d^{opt} indicates the optimized Δ_d . Although ΔE has often been called “condensation energy”, we call it “energy gain” or “energy difference” in this paper, because ΔE does not necessarily correspond to the SC condensation energy measured experimentally, as will be discussed in §3.4.

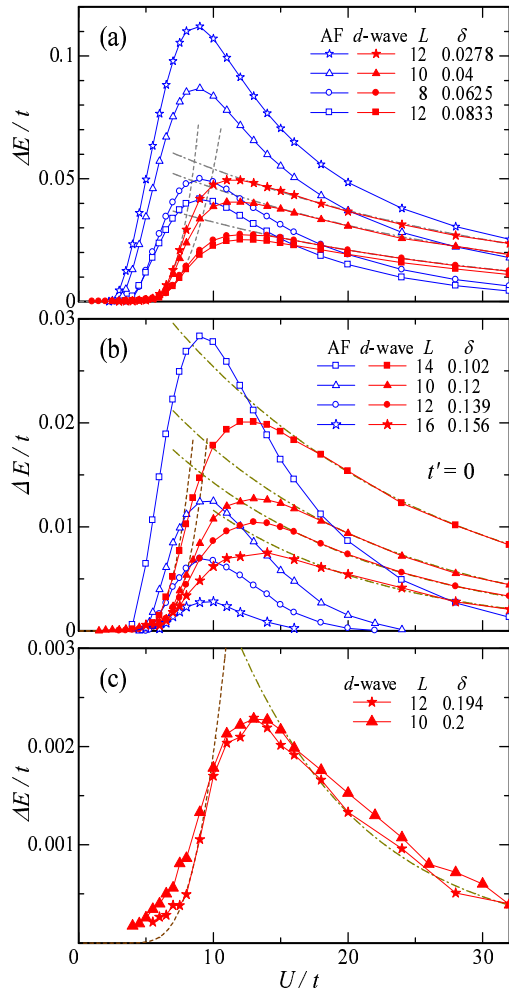


Fig. 3. (Color online) U/t dependences of energy gain $\Delta E/t$ for d -wave (solid symbols) and AF (open symbols) states for $t'/t = 0$. The three panels show different ranges of doping rates: (a) underdoped ($0 < \delta < 0.1$), (b) lightly underdoped to optimum-doped ($0.1 < \delta < 0.16$) and (c) overdoped ($\delta \sim 0.2$) regimes. The AF state is not stabilized for the values of δ in (c). Note that the energy scales are different among the panels. In each panel, the data of the d -wave state are fitted with the functions $\alpha' \exp(-\beta' t/U)$ [dashed lines] on the weak-correlation side ($U < U_{\text{co}}$) and $\alpha \exp(-U/\beta t)$ [dash-dotted lines] on the strong-correlation side ($U > U_{\text{co}}$).

Figure 3 shows the U/t dependences of ΔE in the d -wave state (ΔE^d) and AF state (ΔE^{AF}) defined for Δ_{AF} similarly to eq. (17); panels (a), (b), and (c) show

doped values of δ , respectively. As discussed in ref. 16, ΔE^d is negligible for $U \lesssim 6t$, but abruptly increases as U/t increases, and is roughly fitted as $\Delta E^d/t \sim \alpha' \exp(-\beta' t/U)^{100}$ at approximately $U = W (= 8t)$ (α' , β' : constants). ΔE^d has a maximum at $U \sim U_{\text{co}} = 10t$ – $12t$, then decreases slowly as it is fitted well with the curve

$$\Delta E^d/t = \alpha \exp\left(-\frac{U}{\beta t}\right), \quad (18)$$

for $2W \lesssim U < 4W$. The estimated values of the constants α and β are shown in Fig. 4 as functions of δ . From the form of eq. (18), we consider that the attractive pairing potential in this regime is proportional to $t^2/U (= J/4)$; this indicates that the low-energy physics in this regime is parallel to that of the corresponding t - J -type models.^{16,101} Thus, we conclude that the properties of SC undergo a crossover from a BCS type to an unconventional t - J type at $U \sim U_{\text{co}}$ (this is a loose definition of U_{co}). As long as Ψ_Q^d is SC, this behavior is qualitatively independent of δ , although the magnitude of ΔE^d decreases with δ .

As is evident from eq. (17), ΔE^d originates from a finite d -wave gap. Actually, the behavior of ΔE^d closely corresponds to that of the optimized Δ_d shown in Fig. 5; Δ_d abruptly starts to increase at $U \sim U_c$, where D-H binding also becomes effective, as mentioned.

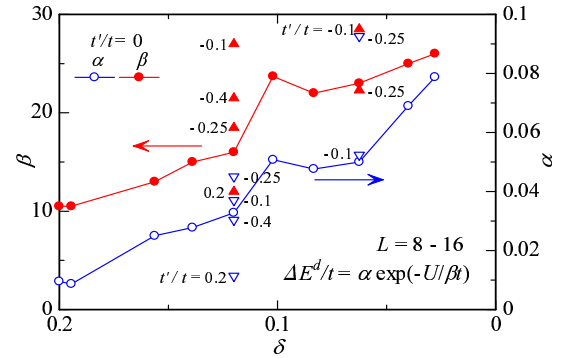


Fig. 4. (Color online) Coefficients α (open symbols) and β (closed symbols) in fitting function of $\Delta E^d/t$ for $U > U_{\text{co}}$ [eq. (18)] as functions of hole density. The circles denote the data for $t'/t = 0$. The data for $t' \neq 0$ (triangles) are included with the values of t'/t .

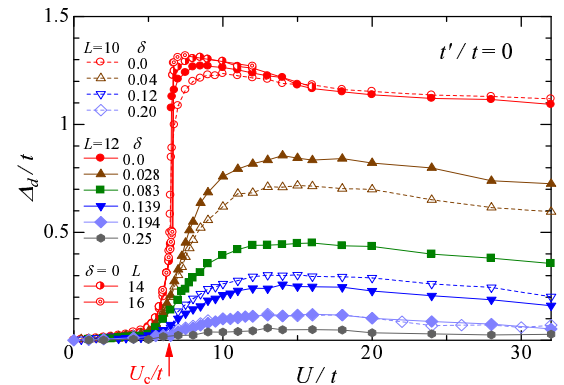


Fig. 5. (Color online) Optimized d -wave gap parameter in Ψ_Q^d as function of U/t for different values of δ (and L).

Now we compare ΔE^d with ΔE^{AF} . As discussed in refs. 16 and 17, ΔE^{AF} is also maximum at $U \sim W$ ($U < U_{\text{co}}$) and has a tail for large U/t . At half filling, ΔE^{AF} is always larger than ΔE^d [Fig. 3 in ref. 16], although ΔE^{AF} decreases rapidly for large U/t . Almost as soon as carriers are doped, ΔE^{AF} is surpassed for large U/t [Fig. 3(a)], and tends to vanish at a certain U/t in the optimally doped region [Fig. 3(b)]. As δ increases, ΔE^{AF} becomes smaller than ΔE^d ($\delta = 0.156$) for any U/t , and finally vanishes for $\delta \sim 0.2$ [Fig. 3(c)]. The phase diagram constructed from these data [Fig. 4(a) in ref. 16] shows that the domain of d -wave SC tends to expand to $\delta = 0$ and that of the AF state shrinks as U/W increases, supporting the result of the t - J model, in which the stable state switches from an AF state to a d -wave state as soon as holes are doped.¹⁵ On the other hand, the AF state seems predominant at $U \sim W$. In fact, however, the AF domain in the phase diagram probably vanishes for $\delta \neq 0$ (unless a d -wave SC order coexists^{67,70}) in accordance with the actual behavior of cuprates, because the AF state for a finite δ is unstable against phase separation, as we will discuss shortly.

Let us turn to the behavior of the components of ΔE ($= \Delta E_t + \Delta E_U$). In Figs. 6(a) and 6(b), the kinetic and interaction parts of ΔE^d are shown as functions of U/t . For small U/t ($\lesssim 10$), the energy gain is derived from the interaction part ΔE_U with a loss in the kinetic part ΔE_t . This mechanism is identical to that of the BCS theory. On the other hand, for large U/t ($\gtrsim 12$), the SC state is stabilized by the reduction in ΔE_t . As discussed in ref. 16, in this regime of U/t , the quasi-particle renormalization factor Z in the nodal direction is enhanced by introducing Δ_d , suggesting that the SC coherence promotes the motion of electrons. In particular, local hoppings that create or annihilate doublons (cf. §3.5) are more enhanced in the SC state. Thus, we conclude that the so-called “kinetic-energy-driven SC” is realized only for $U > U_{\text{co}}$. A FLEX calculation for the Hubbard model also supports this behavior, although U_{co}/t is small and a sharp crossover is not obtained.¹⁰² Because E_t is proportional to the sum of optical conductivity $\sigma_1(\omega)$ (exactly for $t' = 0$),¹⁰³ it is possible that precise optical measurements can determine whether or not cuprates belong to the regime of the t - J model.

Incidentally, similar behaviors of ΔE_U and ΔE_t are found for the AF state as shown in Fig. 7, and for an s -wave SC state in the 2D attractive Hubbard model.⁸⁴ Accordingly, it is possibly a common tendency that nonorder-to-order transitions are induced by the reduction in kinetic energy in strong-correlation regimes.¹⁰⁴

Finally, we discuss possible phase separation. This subject is important in relation to the density modulations or phase separation reported in underdoped cuprates,¹⁰⁵ and has been theoretically pursued mainly using the t - J model with small J/t .¹⁰⁶ A homogeneous state is unstable against phase separation if the charge compressibility

$$\kappa = \frac{1}{n^2} \chi_c = \left(n^2 \frac{\partial^2 E}{\partial n^2} \right)^{-1} \quad (19)$$

is negative, namely, the total energy E/t is convex as

a function of electron density n . In order to check this possibility, we show, in Fig. 8, the total energies of Ψ_Q^d and Ψ_Q^{AF} as functions of δ . For both $U/t = 8$ and 12, the E/t of the d -wave state exhibits a concave curve, namely, $\kappa > 0$, meaning the d -wave state has intrinsic stability. In contrast, the AF state exhibits a convex curve, $\kappa < 0$, indicating that the AF state of partial filling gives rise to a phase separation of the insulating AF state with local filling $\delta = 0$ and a SC (or normal) state with local filling $\delta \gtrsim 0.2$, according to the Maxwell construction. A similar result was reached by a recent QMC study for $t' = 0$.¹⁰⁷ This instability does not occur in electron-doped cases as will be discussed for $t' \neq 0$ in § 4.1 or in the coexistence of the SC and AF orders.^{67,70}

3.3 U/t dependence of correlation functions

To measure the strength of SC, the $d_{x^2-y^2}$ -wave pairing correlation function

$$P_d(\mathbf{r}) = \frac{1}{N_s} \sum_i \sum_{\tau, \tau' = \hat{x}, \hat{y}} (-1)^{1-\delta(\tau, \tau')} \times \langle \Delta_\tau^\dagger(\mathbf{R}_i) \Delta_{\tau'}(\mathbf{R}_i + \mathbf{r}) \rangle \quad (20)$$

is appropriate for the present method. Here, \hat{x} and \hat{y} denote the lattice vectors in the x - and y -directions, respectively, $\delta(\tau, \tau')$ indicates the Kronecker delta, and $\Delta_\tau^\dagger(\mathbf{R}_i)$ is the creation operator of an NN singlet pair at site \mathbf{R}_i ,

$$\Delta_\tau^\dagger(\mathbf{R}_i) = (c_{i\uparrow}^\dagger c_{i+\tau\downarrow}^\dagger + c_{i\uparrow\downarrow}^\dagger c_{i\downarrow}^\dagger) / \sqrt{2}. \quad (21)$$

If $P_d(\mathbf{r})$ remains finite for $|\mathbf{r}| \rightarrow \infty$, a d -wave off-diagonal long-range order exists. As explained in Appendix C, we found a suitable scheme for reliably estimating $P_d(\mathbf{r})$ for $|\mathbf{r}| \rightarrow \infty$ (P_d^∞) from the data of finite L . We confirmed that P_d^∞ converges to zero for Ψ_Q^F and Ψ_Q^{AF} as L increases. Henceforth, we discuss P_d^∞ .

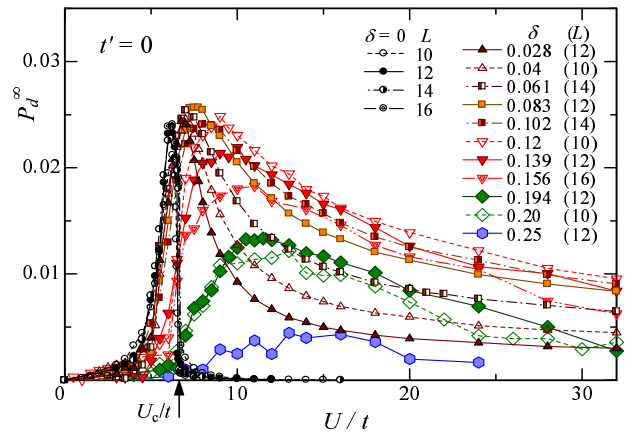


Fig. 9. (Color online) d -wave SC correlation function as function of U/t computed with d -wave states for various doping rates. Circles indicate half filling ($\delta = 0$); similarly, upward triangles (Δ) $\delta \sim 0.03$, squares (\square) $\delta \sim 0.09$, downward triangles (∇) $\delta \sim 0.14$, diamonds $\delta \sim 0.20$, and hexagons $\delta = 0.25$. The arrow indicates the Mott critical value at half filling.

Figure 9 shows the U/t dependence of P_d^∞ calculated with the optimized Ψ_Q^d for some values of δ . The overall

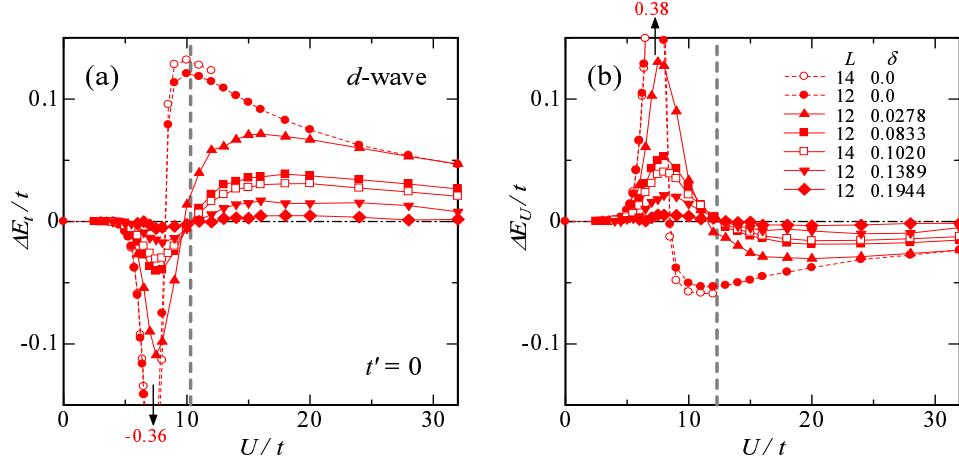


Fig. 6. (Color online) Components [(a) kinetic and (b) interaction parts] of energy gain ΔE^d as functions of U/t . The broad gray dashed lines roughly indicate the points where the signs of ΔE_t and ΔE_U are reversed.

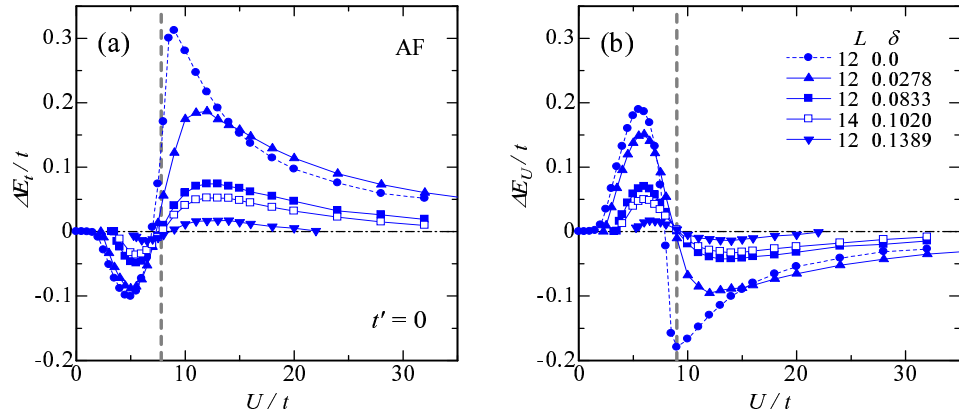


Fig. 7. (Color online) Components [(a) kinetic and (b) interaction parts] of energy gain ΔE^{AF} as functions of U/t . The broad gray dashed lines show the same as those in Fig. 6.

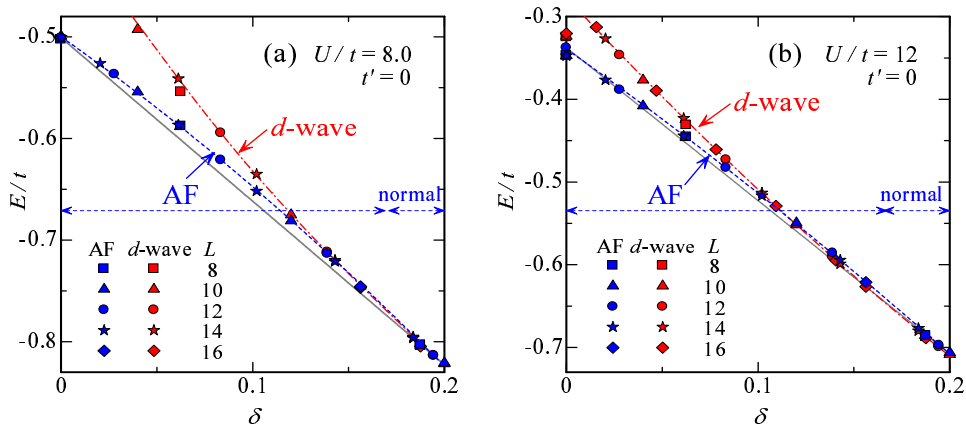


Fig. 8. (Color online) Total energy as function of doping δ of AF and d -wave states for (a) $U/t = 8$ and (b) $U/t = 12$. The AF state is reduced to a normal state for $\delta \gtrsim 0.18$, as shown by horizontal dashed arrows. The solid lines are straight guide lines.

$\Delta E/t$ (Fig. 3), especially for the optimal and overdoped regimes ($\delta \gtrsim 0.15$). A large difference between P_d^∞ and $\Delta E/t$ emerges as δ approaches 0 (e.g., $\delta = 0.028$); P_d^∞ , compared with $\Delta E/t$, decreases rapidly as U/t increases. The extreme case is half filling, at which P_d^∞ vanishes for $U > U_c$, corresponding to the Mott transition, as discussed in ref. 17. Thus, the value of U/t at the maxi-

mum P_d^∞ , which is a better definition of U_{co}/t , decreases to the Mott critical value U_c/t as δ decreases. We leave the analysis of the δ dependence for the next subsection.

For SC in the present case, the spin structure factor

$$S(\mathbf{q}) = \frac{1}{N_s} \sum_{ij} e^{i\mathbf{q} \cdot (\mathbf{R}_i - \mathbf{R}_j)} \langle S_i^z S_j^z \rangle \quad (22)$$

is an important quantity, because the electron pair scattering with $\mathbf{Q} = (\pi, \pi)$ will contribute to the $d_{x^2-y^2}$ -wave pairing. In Fig. 10(a), the U/t dependence of $S(\mathbf{Q})$ calculated with Ψ_Q^d is plotted for six values of δ . As discussed in ref. 17, $S(\mathbf{Q})$ increases with U/t and, in particular, increases discontinuously at U_c/t at half filling in accordance with the first-order Mott transition. For $\delta > 0$, $S(\mathbf{Q})$ still rapidly increases for $U_c \lesssim U \lesssim U_{co}$, although the discontinuity vanishes. The increase in $S(\mathbf{Q})$ for $U < U_{co}$ coincides with the behavior of P_d^∞ , but a further increase in $S(\mathbf{Q})$ for $U > U_{co}$ is opposed to the decrease in P_d^∞ . This is because SC also depends on the mobility of electrons, represented, for example, by the quasi-particle renormalization factor Z [Fig. 6 in ref. 16].

Similar decreasing behavior is found in the charge correlation function between NN sites,

$$N_1 = \left| \frac{1}{4N_s} \sum_{j,\tau} \langle n_j n_{j+\tau} \rangle - n^2 \right|, \quad (23)$$

as shown in Fig. 10(b). Here, τ runs over the four NN sites of site j . N_1 represents NN charge fluctuation and is related to the mobility of electrons. The decrease in N_1 and Z , showing the suppression of charge fluctuation by U/t , resembles the behavior of P_d^∞ for $U > U_c$.

The above argument implies that the strength of SC requires two factors, namely, pair formation owing to AF spin correlation and the fluidity of pairs owing to charge fluctuation. We will argue this topic again in the light of the δ dependence, which is controllable in experiments on cuprates, in the next subsection.

3.4 Doping-rate dependence of various quantities

First, we examine the energy gain of the d -wave state ΔE^d [eq. (17)]. In Fig. 11(a), we show the δ dependence of ΔE^d ; ΔE^d is largest at half filling and monotonically decreases as δ increases for any U/t . Figure 11(b) shows the δ dependence of the optimized d -wave gap Δ_d , which is the sole parameter directly controlling the energy scale

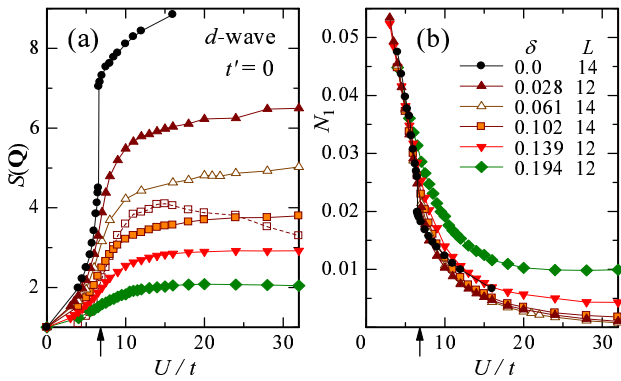


Fig. 10. (Color online) (a) Spin structure factor $S(\mathbf{q})$ at $\mathbf{q} = (\pi, \pi)$ for six electron densities. For comparison, the behavior of the optimized d -wave gap parameter Δ_d/t (exactly $8\Delta_d/t + 1$) is also shown for $\delta = 0.102$ (open squares and dashed line). (b) Nearest-neighbor charge correlation function as function of U/t . The symbols for δ and L are common between the two panels. The arrows indicate the Mott transition point at half filling.

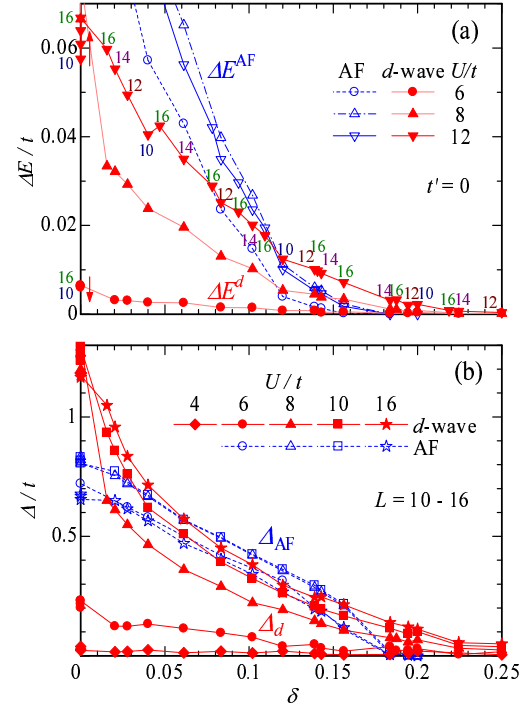


Fig. 11. (Color online) (a) Energy gain $\Delta E/t$ in d -wave and AF states versus doping rate. The numbers near the data points indicate the system sizes (L) used. The arrows alongside the vertical axis denote the direction of the system-size dependence at $\delta = 0$ (downward: $U/t = 6$; upward: $U/t = 8$ and 12). (b) Optimized gap parameters in d -wave (Δ_d) and AF (Δ_{AF}) states as functions of doping rate.

of a singlet gap in Ψ_Q^d . It is natural to consider that Δ_d corresponds to the pseudogap.^{92,108} Δ_d is highly similar to ΔE^d as in the U/t dependence. Thus, we again find that Ψ_Q^d is stabilized by the d -wave singlet formation. We will see the relation of these quantities to the spin correlation shortly.

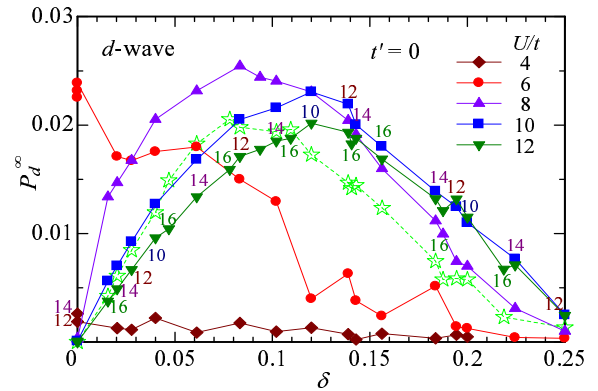


Fig. 12. (Color online) d -wave SC correlation function vs doping rate for several values of U/t in Ψ_Q^d . The numbers (10-16) denote the system sizes L used. The stars denote Δ_{SC}^2 for $U/t = 12$ calculated with eq. (24) using Δ_d obtained by VMC. The magnitude of Δ_{SC}^2 is adjusted to be equal to the corresponding P_d^∞ .

Next, we consider the d -wave SC correlation P_d^∞ ; its δ dependence is shown in Fig. 12. For $U/t = 4$, the magni-

tude of P_d^∞ is very small and has relatively strong L and δ dependences, indicating that firm SC is unlikely to appear for $U/t = 4$. This result is consistent with those of QMC calculations,^{8,9,61} in which the increase in SC correlation as U/t increases is not found for small values of U/t . When U/t is slightly below the Mott transition point U_c/t (~ 7), as in $U/t = 6$, P_d^∞ has the maximum at half filling, and is basically a decreasing function of δ , except for the fluctuation in L (and δ). This strong system-size dependence suggests that the SC is still fragile. These results for $U < U_c$ indicate that T_c does not exhibit a dome shape in the weakly correlated Hubbard model, although the approximate methods claim such behavior.^{6,109}

In contrast, P_d^∞ for $U > U_c$ displays a dome shape as a function of δ , which is caused by the vanishing of P_d^∞ at half filling as a Mott insulator. The shape of P_d^∞ , especially for $U/t = 12$, closely resembles that of the SC order parameter for the NN pairing $|\langle c_{0\uparrow}^\dagger c_{\tau\downarrow}^\dagger \rangle|$ obtained in the t - J model,¹³ and is consistent with the experimental results of T_c and condensation energy in cuprates. For these values of U/t , SC is considered robust owing to the weak system-size dependence. This result indicates that the effective correlation strength in cuprates is high, i.e., $U > U_c$. Thus, high- T_c cuprates are literal “doped Mott insulators”.^{1,4,5}

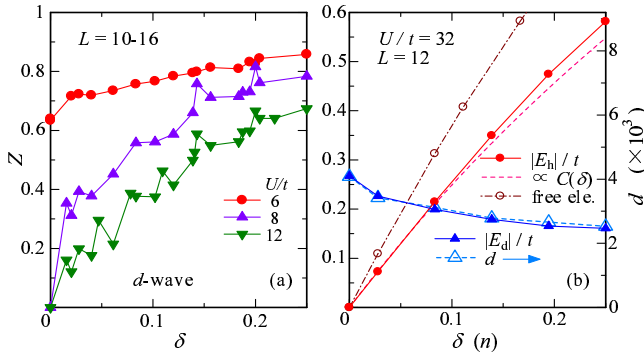


Fig. 13. (Color online) (a) Quasi-particle renormalization factor in nodal direction versus doping rate for d -wave state. (b) Absolute values of E_d and E_h are shown as functions of δ by solid symbols in a strongly correlated case ($U/t = 32$). For comparison, we add the doublon density (open triangles, right axis), a guide line $\propto C(\delta) = 2\delta/(1+\delta)$ (dashed line), and the energy of free electrons as a function of electron density n (open circles).

For $U > U_c$, P_d^∞ increases almost linearly with δ in the underdoped regime, in contrast to quantities such as Δ_d/t and $\Delta E^d/t$, which are monotonically decreasing functions of δ . As mentioned, this is because the strength of SC depends on two factors, singlet-pair formation (Δ_d) and quantities related to charge transport such as carrier density and the mobility of carriers. The latter quantities are bound to increase as δ increases for $U > U_c$, being released from the suppression of charge fluctuation in Mott insulators. As an example, in Fig. 13(a), we show the quasi-particle renormalization factor Z estimated from the jumps in $n(\mathbf{k})$ in the nodal direction. Since Z roughly represents the inverse effective mass, Z is zero at half filling and monotonically increases as δ increases.

t - J model.¹⁰⁸ N_1 [eq. (23)] and the conductive part of E_t discussed in §3.5 [$|E_h|$ in Fig. 13(b)] are also increasing functions of δ .

To consider the δ dependence of SC strength, it is useful to mention a simple analytic calculation. In a pioneering study using a Gutzwiller-type approximation for the t - J model,⁹² the relation

$$\Delta_{\text{SC}} = \frac{2\delta}{1+\delta} \Delta_d \quad (24)$$

was derived; here, the energy scale of SC (Δ_{SC}) originates solely from Δ_d (d -wave singlet gap) but is modified by the factor of the carrier density. As an example, we estimate Δ_{SC}^2 for $U/t = 12$ using Δ_d calculated by VMC, and the result is plotted in Fig. 12 by open stars. Δ_{SC}^2 qualitatively agrees with P_d^∞ for $U/t = 12$. A similar dome shape is also obtained from $Z\Delta_d$, instead of eq. (24). Note that in slave-boson-mean-field theory,^{4,110} T_c in the underdoped regime is determined by the Bose condensation temperature T_B ($\propto \delta$) of holons, which represent the charge part of carriers.

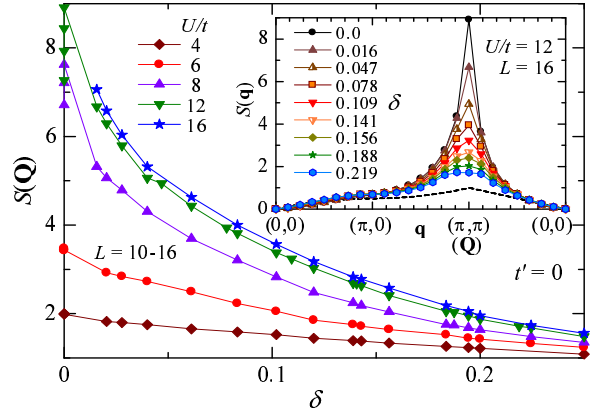


Fig. 14. (Color online) Spin structure factor at $\mathbf{q} = (\pi, \pi)$ in d -wave state as function of doping rate for five values of U/t . The inset represents $S(\mathbf{q})$ at $U/t = 12$ for various doping rates along the path $(0,0) \rightarrow (\pi,0) \rightarrow (\pi,\pi) \rightarrow (0,0)$. The dashed line shows the case of $U = 0$ and $\delta = 0$.

We turn to the spin structure factor $S(\mathbf{q})$. In the inset of Fig. 14, $S(\mathbf{q})$ of Ψ_Q^d at $U/t = 12$ is depicted for various δ . The sharp peak at $\mathbf{q} = \mathbf{Q}$ near half filling confirms a predominant AF spin correlation, and $S(\mathbf{q})$ preserves the maximum at \mathbf{Q} for $\delta \lesssim 0.2$. The main panel of Fig. 14 shows the δ dependence of $S(\mathbf{Q})$ for five values of U/t ; $S(\mathbf{Q})$ is a decreasing function of δ for any correlation strength. The small system-size dependence indicates the short-range nature of $S(\mathbf{Q})$. We here reiterate the close connection between the spin correlation and the D-H binding correlation (Fig. 2); the δ dependences of ΔE^d , Δ_d , and $S(\mathbf{Q})$ closely resemble one another. This suggests a strong correlation between Δ_d and the AF spin correlation, namely, the energy of Ψ_Q^d is probably reduced by the formation of d -wave singlet pairs through the AF spin correlation.

Now, we discuss how spin and charge density gaps evolve when δ is introduced. It was revealed in ref. 17 for half filling that Ψ_Q^d has a finite spin (SC) gap for

any positive U/t , but is gapless for $U < U_c$ and gapped for $U > U_c$ in the charge sector. It is known within the single-mode approximation¹¹¹ that a charge density gap opens [closes] if the charge density structure factor

$$N(\mathbf{q}) = \frac{1}{N_s} \sum_{i,j} e^{i\mathbf{q} \cdot (\mathbf{R}_i - \mathbf{R}_j)} \langle n_i n_j \rangle - n^2 \quad (25)$$

behaves as $N(\mathbf{q}) \propto |\mathbf{q}|^2$ [$\propto |\mathbf{q}|$] for $|\mathbf{q}| \rightarrow 0$. For the spin sector, a similar treatment with $S(\mathbf{q})$ is available. In Fig. 15, we show small- $|\mathbf{q}|$ behaviors of $S(\mathbf{q})$ and $N(\mathbf{q})$ at $U = 12t$ ($> U_c$) for various doping rates. An SC (singlet) gap survives up to the overdoped regime ($\delta > 0.15$), although the quadratic feature of $S(\mathbf{q})$ becomes less distinctive as δ increases. On the other hand, in $N(\mathbf{q})$, the quadratic behavior immediately disappears upon doping, namely, the charge density gap vanishes for $\delta > 0$, because $|\mathbf{q}|^2/N(\mathbf{q})$ seems to vanish for $|\mathbf{q}| \rightarrow 0$.

Let us summarize the energy scales deduced from the present calculations (Fig. 16). The gap scales representing the features of SC for $U > U_c$ are classified into two kinds: (i) Quantities exclusively related to the singlet formation, which is derived from the superexchange interaction, monotonically decrease by doping, which weakens the AF correlation. They are symbolically indicated by Δ_d in Fig. 16. (ii) Quantities directly related to SC, which

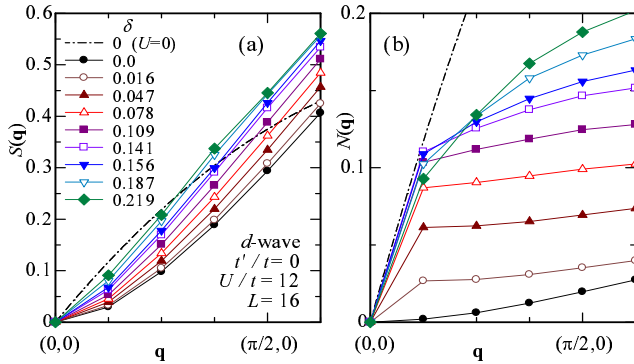


Fig. 15. (Color online) Small- $|\mathbf{q}|$ behaviors of (a) spin and (b) charge density structure factors in $(0,0)$ - $(\pi,0)$ direction for $U/t = 12$ and some doping rates. In (b), $N(|\mathbf{q}|) \propto |\mathbf{q}|^\gamma$ with $\gamma \leq 1$ for $\mathbf{q} \rightarrow 0$ seems to hold for $\delta > 0$. The system used and symbols of δ are common to the two panels.

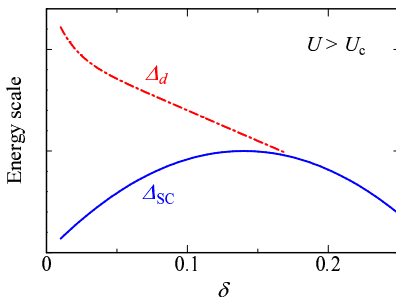


Fig. 16. (Color online) Schematic δ dependence of two kinds of gap scales deduced from present calculations for $U > U_c$.

is affected by both the singlet gap Δ_d and charge transportability, increase as δ increases in the underdoped regime, as shown by Δ_{SC} . It is natural to substitute T_c (T_{pair}) for Δ_{SC} (Δ_d) in Fig. 16.

Finally, we touch on the relation between ΔE^d in eq. (17) and the SC condensation energy experimentally observed (ΔE_{cond}). In the BCS theory, ΔE^d coincides with ΔE_{cond} at $T = 0$. However, this relation is not applicable to the present case, because only a part of Δ_d contributes to Δ_{SC} and the residual part remains as an incoherent singlet gap. Actually, values ΔE_{cond} estimated from the specific heat measurement^{112,113} exhibit a dome shape as a function of δ , similarly to T_c , which is completely different from the monotonic behavior of ΔE^d shown in Fig. 11(a). Ideally, the above incoherent part should cancel with the corresponding part of a proper normal state; thus, an improvement of the normal state is necessary. Anyway, we should be prudent in comparing ΔE^d with ΔE_{cond} .

3.5 Mechanism of conduction

In this subsection, we argue that a feature of DC conduction undergoes a marked change through crossover. Here, we aim to obtain an intuitive picture of conduction within the scope of kinetic energy E_t rather than to have a quantitative discussion using a direct measure such as the Drude weight. To this end, it is useful to analyze the kinetic energy, by dividing it into two components, $E_t = E_d + E_h$, as the hopping process varies (E_d) or does not vary (E_h) the number of doublons,¹¹⁴ as shown in Fig. 17(a). E_d is derived from the hopping processes that create and destroy D-H pairs, and corresponds to the J term in the t - J model. E_h comes from the direct hopping of holons and doublons, which corresponds to the t term in the t - J model.¹¹⁵ In Fig. 17(b), we plot E_d and E_h as functions of U/t for several δ . The behavior of the two components clearly changes at approximately U_{co}/t .

We begin with the strongly correlated regime ($U > U_{co}$). At half filling, E_h substantially vanishes in the Mott insulating regime ($U > U_c$); E_d remains finite and behaves proportionally to $-4t^2/U$ ($= -J$). Since the state is insulating, E_d here does not contribute to current, namely, local processes that create and annihilate D-H pairs are only repeated. They correspond to the large- ω part in $\sigma_1(\omega)$: transitions between the lower and upper Hubbard bands. When carriers are doped, this behavior of E_d ($\propto -J$) is basically unchanged; its magnitude decreases slowly as δ increases, accurately corresponding to a decrease in doublon number, as shown in Fig. 13(b). Thus, the local D-H processes at $\delta = 0$ remain intact for $\delta > 0$, meaning that E_d is not involved in conduction or itinerancy. On the other hand, E_h becomes finite and is still almost constant for $U > U_{co}$ with the magnitude linear in δ or $\propto 2\delta/(1+\delta)$ in eq. (24), as depicted in Fig. 13(b). This indicates that the independent motion of doped holons is realized for $U > U_{co}$, although their mass is somewhat heavier than that of the free electrons.¹¹⁶ It follows that two kinds of holons play entirely different roles in SC, namely, the holons created as D-H pairs de-

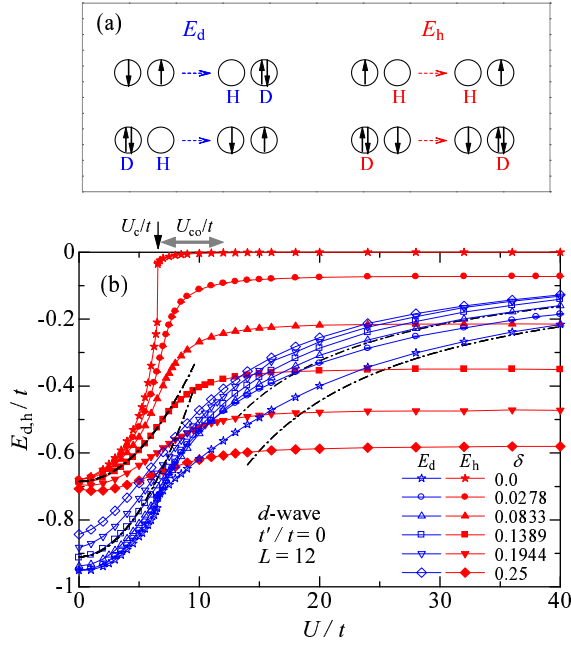


Fig. 17. (Color online) (a) Hopping processes that contribute to the two components of kinetic energy, E_d and E_h , are schematically shown. (b) The U/t dependences of E_d and E_h are shown for six doping rates. The two dash-dotted lines in the small- U/t [large- U/t] regime are guides as $\sim (U/t)^2 + \text{const.}$ for $\delta = 0.1389$ [$\sim -t/U = -J/(4t)$ in E_d for $\delta = 0$ and 0.0833].

vote themselves to forming local singlet pairs, whereas the holons introduced by doping act as current carriers, as schematically sketched in Fig. 18(b). Thus, the number of doped holes is equal to the number of carriers, which will make a small quasi-Fermi surface such as a Fermi arc or pocket. This feature is simply that of the t - J model,⁵ and consistent with various experiments on cuprates,¹¹⁷ and supports the very low superfluid densities.¹¹⁸ The residual (background) spinons (singly occupied sites) remain localized unless the doped holons collide with them; this fact is possibly related to the recent observed neutron scattering for Bi2212,¹¹⁹ which indicated that the source of the magnetic response in doped cuprates is localized spins.

In contrast, for $U < U_{co}$, both E_d and E_h behave as

$$E_d \sim c_d U^2/t + E_d(0),$$

$$E_h \sim c_h U^2/t + E_h(0),$$

with c_d and c_h being constants, as shown in Fig. 17(b). This common behavior indicates that every hopping process contributes to E_t in the same way. Since the D-H binding is ineffective in this regime, holons cannot be classified into the two kinds, and all electrons can contribute to conduction, as in Fig. 18(a), resulting in a large (ordinary) Fermi surface with a carrier number of N . Correspondingly, the number of doped holes is not in agreement with the carrier number, in contrast to the experimental results on cuprates.

We have also obtained results similar to those in Fig. 17(b) for the normal and AF states, although they are not shown here. The mechanism of conduction in doped Mott insulators is entirely different from that in weakly correlated systems.

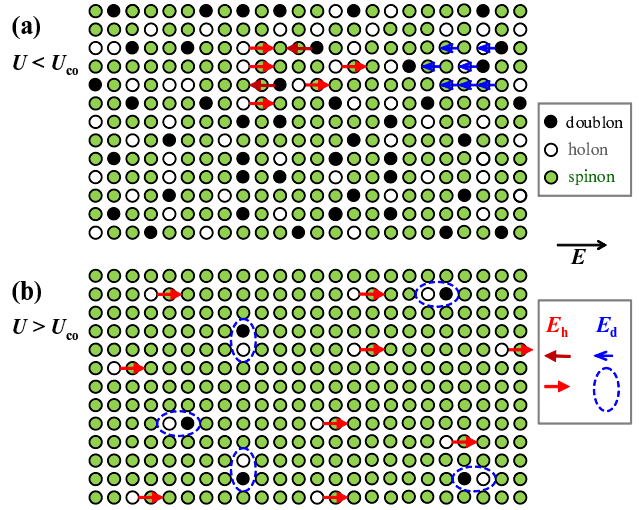


Fig. 18. (Color online) Mechanism of conduction is schematically compared between (a) the weakly correlated [Fermi liquid or BCS-type SC] regime and (b) the strongly correlated [doped Mott insulator] regime. Small arrows represent the motion of particles if a field (\vec{E}) is applied; in (a) arrows are drawn only for a small number of particles for clarity. The dashed ellipses in (b) indicate the local creation and annihilation processes of bound D-H pairs, which do not contribute to current.

4. Effect of Diagonal Transfer t'

In this section, we study the effect of next-nearest-neighbor hopping (t'), which is the principal term for characterizing the individuality of each high- T_c cuprate. In §4.1, we consider the stability of Ψ_Q^d against Ψ_Q^{AF} in introducing t' and possible phase separation near half filling. In §4.2, we discuss the origin of the stability of the d -wave and AF states on the basis of the effect of t' . In §4.3, we study the effect of t'/t on P_d^∞ , whereby we discuss the mechanism of enhancing P_d^∞ .

4.1 Energy gain by d -wave gap

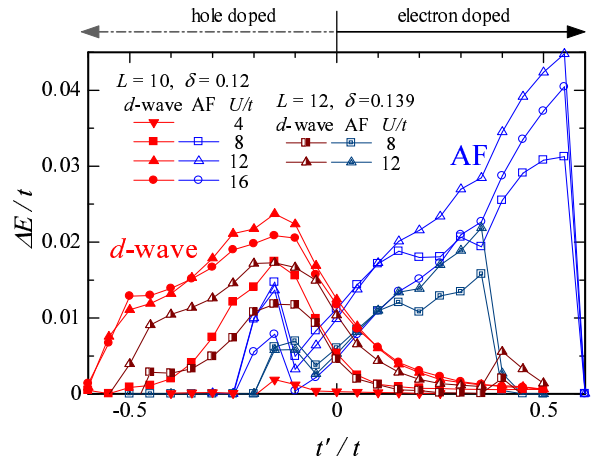


Fig. 19. (Color online) Energy gains for d -wave (solid and half-solid symbols) and AF (open and double-line symbols) states as functions of t'/t for optimally doped densities. For comparison, data for some values of U/t and two values of L are plotted.

At half filling, we now focus on the range $t'/t < 0$.

because there is symmetry between t' and $-t'$, as discussed in ref. 17 and Appendix A. Upon doping carriers, however, this symmetry is broken. Figure 19 shows ΔE^d and ΔE^{AF} for some values of U/t as functions of t'/t at roughly optimally doped densities $\delta = 0.12$ and 0.139 . In the hole-doped cases ($t'/t < 0$), ΔE^d tends to be enhanced, and ΔE^{AF} is suppressed. For $U/t \geq 8$, ΔE^d has a broad maximum in the range $-0.3 \lesssim t'/t \lesssim -0.1$, and tends to vanish relatively rapidly for $t'/t \lesssim -0.45$. In contrast, ΔE^{AF} vanishes except for a small peak at $t'/t \sim -0.15$. This peak is caused by the overlap of the Fermi surface with flat-band parts near $(\pi, 0)$, as we will discuss later for Ψ_Q^d . In the electron-doped cases ($t'/t > 0$), the situation is opposite. ΔE^d gradually and monotonically decreases as t'/t increases, whereas ΔE^{AF} monotonically increases until the sudden breakdown at a large t'/t .

The U/t dependences (not shown) of ΔE^d and ΔE^{AF} are qualitatively similar to those for $t' = 0$ in Fig. 3, although the overall amplitude depends on t'/t as in Fig. 19.

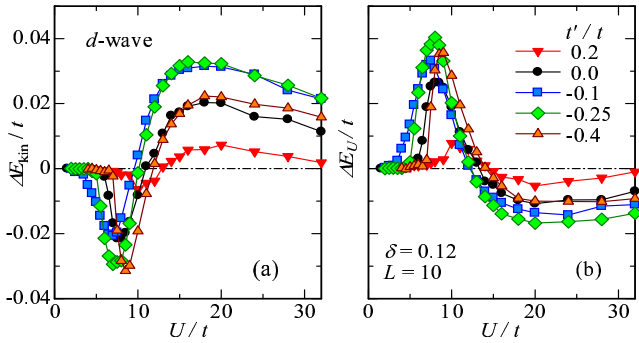


Fig. 20. (Color online) (a) Kinetic and (b) interaction parts of energy gain ΔE^d for various values of t'/t as functions of U/t .

We touch on the components of the energy gain ΔE for finite t'/t . In Figs. 20(a) and 20(b), we plot the kinetic (t and t' terms) and interaction parts of ΔE , respectively, as functions of U/t . The behaviors of the two components are qualitatively identical to those for $t' = 0$ (Fig. 6): SC is induced by the reduction in interaction (kinetic) energy for small (large) values of U/t . Here, the doping rate is fixed at $\delta = 0.12$, but the tendency is unchanged for other δ . For small $|t'/t|$, the sum of $\sigma_1(\omega)$ becomes approximately proportional to the kinetic energy ($-E_{\text{kin}}$).

In §3.2, we showed that Ψ_Q^{AF} is unstable against phase separation for $t' = 0$ (Fig. 8). Here, we discuss the tendency toward the phase separation for $t' \neq 0$. In Fig. 21, we plot the total energy of the AF and d -wave states as functions of δ for hole- and electron-doped cases. For Ψ_Q^d , E^d/t is concave ($\kappa > 0$) for both values of t'/t , indicating that the d -wave state is still stable if t' is added, regardless of the kind of doped carriers. For the AF state, it becomes slightly concave for $t'/t = 0.2$ (electron-doped case) [Fig. 21(b)], indicating that the commensurate AF state is intrinsically stable for electron doping. On the other hand, E^{AF}/t is still convex ($\kappa < 0$) for $t'/t = -0.10$ (hole-doped case), indicating that the commensurate AF state is still stable for hole doping.

ΔE_{AF} ($0 < \delta \lesssim 0.15$) [Fig. 21(a)]. Thus, for hole doping, a phase separation occurs in the underdoped regime as in $t' = 0$. Such behavior is almost independent of U/t when U/t is sufficiently large; the same behavior has been found for the t - J model.¹²⁰

The reason for the instability of the AF state seems trivial; doping rapidly deteriorates the nesting of the Fermi surface for $t'/t < 0$, in contrast to the case of $t'/t > 0$. Although we have to be careful in directly comparing the present result with experiments, because the band renormalization effect is not explicitly introduced in Ψ_Q^d or Ψ_Q^{AF} , there are some suggestive experiments: A neutron scattering experiment in very lightly doped $\text{La}_{2-x}\text{Sr}_x\text{CuO}_4$ with $x < 0.02$ ¹²¹ found a phase separation to a commensurate AF ordered phase and a spin-glass phase. On the other hand, such a phase separation does not appear in electron-doped $\text{Pr}_{1-x}\text{LaCe}_x\text{CuO}_4$.^{121, 122}

4.2 Origin of t' -dependence regarding stability of d -wave and AF states

The t'/t dependences of ΔE^d and ΔE^{AF} in the optimally doped regime (Fig. 19) are basically unchanged even if δ varies, as shown in Fig. 22 for $U/t = 12$. For $t'/t = 0.2$ (solid symbols), we have $\Delta E^{\text{AF}} > \Delta E^d$ for any δ ; for $t'/t = 0$ (half solid symbols) and -0.1 (double-line symbols), ΔE^{AF} and ΔE^d interchange at $\delta \sim 0.89$ and 0.91 , respectively, whereas for $t'/t = -0.25$ (open symbols), we always have $\Delta E^{\text{AF}} < \Delta E^d$. Thus, the range of δ where Ψ_{AF} (Ψ_d) is predominant rapidly shrinks as $|t'/t|$ increases on the hole- (electron-)doped side. Incidentally, ΔE^{AF} remains small near half filling for $t'/t = 0.2$ and -0.25 . This is probably because the renormalization of the Fermi surface is not explicitly introduced in Ψ_Q^{AF} ; this effect becomes decisive for $\delta \rightarrow 0$ to retrieve the nesting condition.^{123, 124} We expect $\Delta E^{\text{AF}} > \Delta E^d$ for $\delta \sim 0$ even for large $|t'/t|$ in improved wave functions.

On the basis of Figs. 19 and 22, let us consider the stability of the d -wave and AF states with respect to t'/t . As $|t'/t|$ increases, the curvature of the Fermi surface in Φ_{F} becomes more concave in the nodal direction $(0, 0)$ - (π, π) , as shown in the inset of Fig. 22. Furthermore, it is expected that the scattering with $\mathbf{q} = \mathbf{Q}$ is activated in the area of doped Mott insulators, as discussed in §3.3 and §3.4.

First, we discuss the origin of stability of Ψ_Q^{AF} . In the electron-doped cases, the nesting does not deteriorate rapidly when δ increases away from half filling, namely, the Fermi surface continues to largely overlap with the magnetic Brillouin zone boundary as a whole, as shown in the inset of Fig. 22. The effect of a large density of states near $(\pi, 0)$ [see Fig. 23] is subsidiary for Ψ_Q^{AF} . On the other hand, the Néel order disappears rather suddenly when t'/t becomes excessively large or when holes are doped, because the above overlap suddenly vanishes. Incidentally, the band renormalization effect becomes important for the AF order for $U > W$;^{88, 124} we will reconsider this subject in future publications.

In contrast, conceivable reasons why the d -wave favors finite negative values of t'/t are as follows: (i) Because the band renormalization effect is not explicitly introduced in Ψ_Q^d , the Fermi surface is not renormalized, and the nesting is not deteriorated by doping.

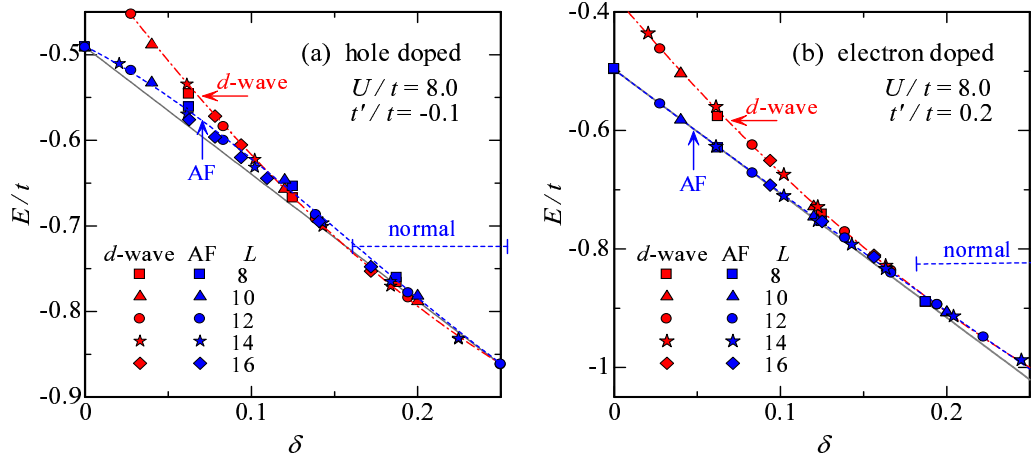


Fig. 21. (Color online) Total energy of d -wave (Ψ_Q^d) and AF (Ψ_Q^{AF}) states as functions of doping rate. In (a) and (b), hole-doped ($t'/t < 0$) and electron-doped ($t'/t > 0$) cases are plotted, respectively. The data for several system sizes are fitted by the method of least squares, and shown with dashed (AF) and dash-dotted (d -wave) lines. The gray solid lines are straight guide lines in the AF case. In the region indicated by ‘normal’, the optimized AF state is reduced to the normal state, namely, $\Delta_{AF} = 0$. In (b), we omit the data of Ψ_Q^{AF} in the vicinity of half filling owing to the breakdown of the AF phase (see text). Similar data for $t' = 0$ are given in Fig. 8.

maximum in the antinodal (k_x and k_y) directions, the energy gain is large when the electrons near $(0, \pi)$ and $(\pi, 0)$ are occupied. (ii) In the noninteracting case, the \mathbf{k} -dependent density of states, $1/|\nabla\epsilon(\mathbf{k})|$, is minimum in the nodal direction including $(\pi/2, \pi/2)$, but becomes large near the antinodal points $(\pi, 0)$ and $(0, \pi)$ owing to the band flatness. Actually, as shown by the dashed line in Fig. 23, $1/|\nabla\epsilon(\mathbf{k})|$ becomes large especially for $t'/t = -0.3$ as \mathbf{q} approaches $(\pi, 0)$ from $(0, 0)$. (iii) The vector \mathbf{Q} connects two \mathbf{k} points near the magnetic Brillouin zone boundary including the antinodal points with mutually inverse signs of $\Delta_{\mathbf{k}}$. Thus, Ψ_Q^d can take advantage of the

d -wave pair scattering of \mathbf{Q} near the antinodal points. We will pursue this topic in §4.3 and §5.

This feature of Ψ_Q^{AF} and Ψ_Q^d is reflected in the behavior of the momentum distribution function

$$n(\mathbf{k}) = \frac{1}{2} \sum_{\sigma} \langle c_{\mathbf{k}\sigma}^{\dagger} c_{\mathbf{k}\sigma} \rangle. \quad (26)$$

Figure 23 shows a comparison of $n(\mathbf{k})$ among the optimized d -wave, AF, and normal states for an underdoped density. The $n(\mathbf{k})$ of the normal state exhibits clear discontinuities (Fermi surface) near $(\pi, 0)$ and $(\pi/2, \pi/2)$. Near $(\pi, 0)$, the $n(\mathbf{k})$ of both d -wave and AF states are considerably changed from that of the normal state, indicating that scattering actively takes place there. Near $(\pi/2, \pi/2)$, the $n(\mathbf{k})$ of the AF state is again noticeably modified depending largely on t'/t , but the $n(\mathbf{k})$ of the

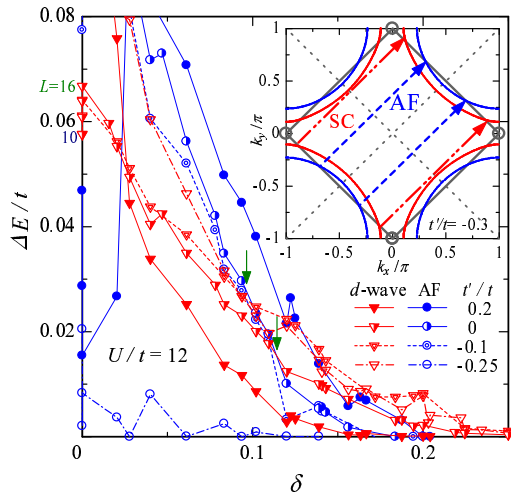


Fig. 22. (Color online) Comparison of energy gain between d -wave (triangles) and AF (circles) states as function of doping rate for four t'/t and $U/t = 12$. The arrows indicate the crossing points of ΔE^{AF} and ΔE^d for $t'/t = 0$ and -0.1 . Systems of $L = 10$ -16 are used. The inset shows the Fermi surface in the electron picture for $n = 0.85$ (favored by d -wave) and 1.10 (favored by AF) for $t'/t = -0.3$. The arrows are the \mathbf{Q} vectors connecting the hot spots [intersections of the Fermi surface and magnetic Brillouin zone boundary indicated by the gray bold line]. The gray dotted lines indicate the nodes of the d -wave state, and the gray circles the van Hove singularity points near the Fermi surface.

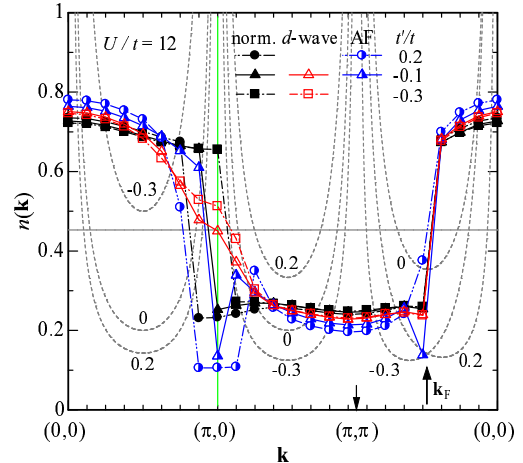


Fig. 23. (Color online) The momentum distribution functions are compared among the d -wave (open symbols), AF (half closed), and normal (closed) states for three values of t'/t , $\delta = 0.094$ and $L = 16$. Firm orders exist for the d -wave and AF states. The gray horizontal line shows $n/2$. The gray dashed curves represent the relative magnitude of the noninteracting \mathbf{k} -dependent density of states $1/|\nabla\epsilon|$ for three values of t'/t .

d -wave state changes only slightly, and is almost independent of t'/t . Now, we are certain that, for Ψ_Q^d , the scattering of \mathbf{Q} is ineffective in the nodal direction, but relevant near the antinodal points.

4.3 d -wave pairing correlation

We turn to the d -wave SC correlation function in Ψ_Q^d . In Fig. 24, the U/t dependence of P_d^∞ , defined by eq. (20) and in Appendix C, is shown for four finite values of t'/t . In Fig. 25, the δ dependence of P_d^∞ is shown for four values of U/t . Although the overall behavior is similar to that in the case of $t' = 0$ (Figs. 9 and 12), there are noteworthy differences owing to the effect of t' . (i) The magnitude of P_d^∞ is somewhat enhanced for $t'/t = -0.1$ and -0.25 , but is suppressed for $t'/t = 0.2$, in accordance with the behavior of ΔE^d discussed in §4.1. (ii) For $U > U_c$, the doping rate giving the maximum P_d^∞ for a fixed U/t shifts to the overdoped side as t'/t decreases. (iii) For $t'/t = -0.1$, P_d^∞ starts to increase at a smaller U/t . (iv) Although we do not show detailed data in Fig. 24, for $t'/t \lesssim -0.4$ and $\delta \gtrsim 0.2$, a state with a large P_d^∞ is competitive with a state with a tiny P_d^∞ ($\Delta_d/t \sim 0$), suggesting that the SC state collapses at approximately these parameters.

First, let us consider points (i) and (ii) in the strongly correlated regime. As in Fig. 25(d), for $U(=12t)$ sufficiently larger than U_c , P_d^∞ forms a well-proportioned dome shape as a function of δ . This δ dependence of P_d^∞ is consistent with those of T_c and condensation energy observed in cuprates. We define δ_{\max} as the value of δ that gives the largest P_d^∞ for given U/t and t'/t . For $\delta < \delta_{\max}$, P_d^∞ is proportional to δ and is almost independent of t'/t and L . This means that SC in the underdoped regime is steady, and the magnitude of P_d^∞ depends only on U/t , and not on minute band structures. On the other hand, for $\delta > \delta_{\max}$ in the hole-doped cases ($t'/t < 0$), P_d^∞ irregularly depends on t'/t and L , and is scattered to some extent.¹²⁵ Thus, the strength of SC is sensitive to the shape of the Fermi surface and fragile in the overdoped regime. However, P_d^∞ becomes larger than that for $t' = 0$, probably because the t' term bends the Fermi surface so that it may pass by the antinodal points. Similar behavior has been observed for the t - J model.^{51,88} In the electron-doped case, δ_{\max} is smaller than those in the hole-doped cases, but the fluctuation with respect to δ and L is small for $\delta > \delta_{\max}$, so that SC is steady. In the transitional regime [Fig. 25(c) for $U_c < U \lesssim U_{co}$], although P_d^∞ manages to preserve its dome shape, δ_{\max} is reduced to have a wide irregular range for $t'/t < 0$. In the electron-doped case ($t'/t = 0.2$), P_d^∞ is suppressed compared with when $t'/t = 0$ and almost vanishes in the overdoped regime. Some similar features were pointed out in a recent study by Tocchio *et al.*¹²⁶

Next, we look at the case of intermediate correlation strength [$U = 6t$, Fig. 25(b)], which is slightly smaller than the Mott critical value U_c . As discussed in ref. 17, P_d^∞ for $t' = 0$ exhibits a sharp peak immediately below U_c ($\sim 7t$) at half filling; such behavior is unchanged for $t' \neq 0$ (circle symbols in Fig. 24). Because $U/t = 6$ is close to this peak value, P_d^∞ is practically the largest

particular, for $t'/t = -0.4$ and 0.2 , P_d^∞ almost vanishes for $\delta > 0.05$. Similarly to the case of $t' = 0$, the behavior of P_d^∞ here is contradictory to the dome shape of T_c and the condensation energy observed in cuprates, in contrast to the cases of $U > U_c$.

Now we move to point (iii) regarding small values of U/t . As discussed in §3.3 for $t' = 0$, P_d^∞ is negligible for U/t as small as 4. As shown in Fig. 24, this feature basically does not alter even if t' is added, except for when $t'/t = -0.1$ [Fig. 24(a)]. This exceptional enhancement of P_d^∞ is evident in Fig. 25(a), where appreciable magnitude appears only for $t'/t = -0.1$ among the six values of t'/t . We argue in the following that this exceptional increase in P_d^∞ at $t'/t \sim -0.1$ for a small U/t is useful to infer the origin of SC.

In Fig. 26, we show P_d^∞ for $U/t = 4$ with star symbols as a function of t'/t for four δ . The meaningful magnitude of P_d^∞ is limited to a narrow range of $-0.16 \lesssim t'/t \lesssim -0.075$ for underdoped densities [Figs. 26(a) and 26(b)] and similarly a narrow range of $-0.275 \lesssim t'/t \lesssim -0.075$ for an overdoped density, $\delta = 0.1944$ [Fig. 26(d)]. These results are consistent with those of a recent QMC study,⁶¹ which showed that the SC susceptibility vanishes for $t' = 0$ but remains finite for $t'/t = -0.2$ for $U/t \leq 5$ in the optimally doped regime. In Fig. 26, we simultaneously plot the momentum distribution function $n(\mathbf{k})$ calculated with Ψ_Q^F and Ψ_Q^d at a couple of available \mathbf{k} points near the antinodal point $\pi(1, 0)$, i.e., $\mathbf{X} = \pi(1, \frac{1}{L})$ and $\mathbf{X}' = \pi(1 - \frac{2}{L}, \frac{1}{L})$. As t'/t is increased, $n(\mathbf{X})$ or $n(\mathbf{X}')$ of Ψ_Q^F discontinuously drops from near unity to near zero when the Fermi surface passes through the \mathbf{X} or \mathbf{X}' point, as indicated by arrows on the upper axes. Note that, in each panel, the positions of the peak and shoulders of P_d^∞ precisely coincide with those at which the Fermi surface overlaps with antinodal \mathbf{k} points. As in Fig. 23, $(\pm\pi, 0)$ and $(0, \pm\pi)$ are van Hove singularity points for $|t'/t| \leq 0.5$, and connected to one another by the AF vectors $\mathbf{Q} = (\pi, \pm\pi)$, $(\pm\pi, \pi)$. It follows that the pair scattering with \mathbf{Q} and SC are enhanced at the values of t'/t indicated by the arrows. This SC mechanism is consistent with the d -wave BCS theory.¹²⁷

However, the mechanism for small values of U/t has difficulties in explaining the features of high- T_c cuprates. First, the effective values of t'/t of cuprates show a relatively wide range; single-layer La systems and double-layer Y and Bi systems have $t'/t \sim -0.1$ and -0.3 , respectively.^{46–50} However, the above SC mechanism sensitively depends on t'/t or the band structure, and the SC correlation is enhanced only in the limited range. It is unlikely that robust SC occurs at $t'/t = -0.3$ in the whole relevant range of δ . Second, it is probable that the magnitude of P_d^∞ discussed above is much weaker. As shown in Fig. 25(a), P_d^∞ has a large and relatively regular system-size dependence, and consequently seems to become negligible for $L \rightarrow \infty$.

For comparison, we preform the same analysis in a strongly correlated case, $U/t = 12$ (Fig. 27). In the underdoped regime [panels (a) and (b)], P_d^∞ has appreciable magnitudes in a wide range of t'/t , and the t'/t

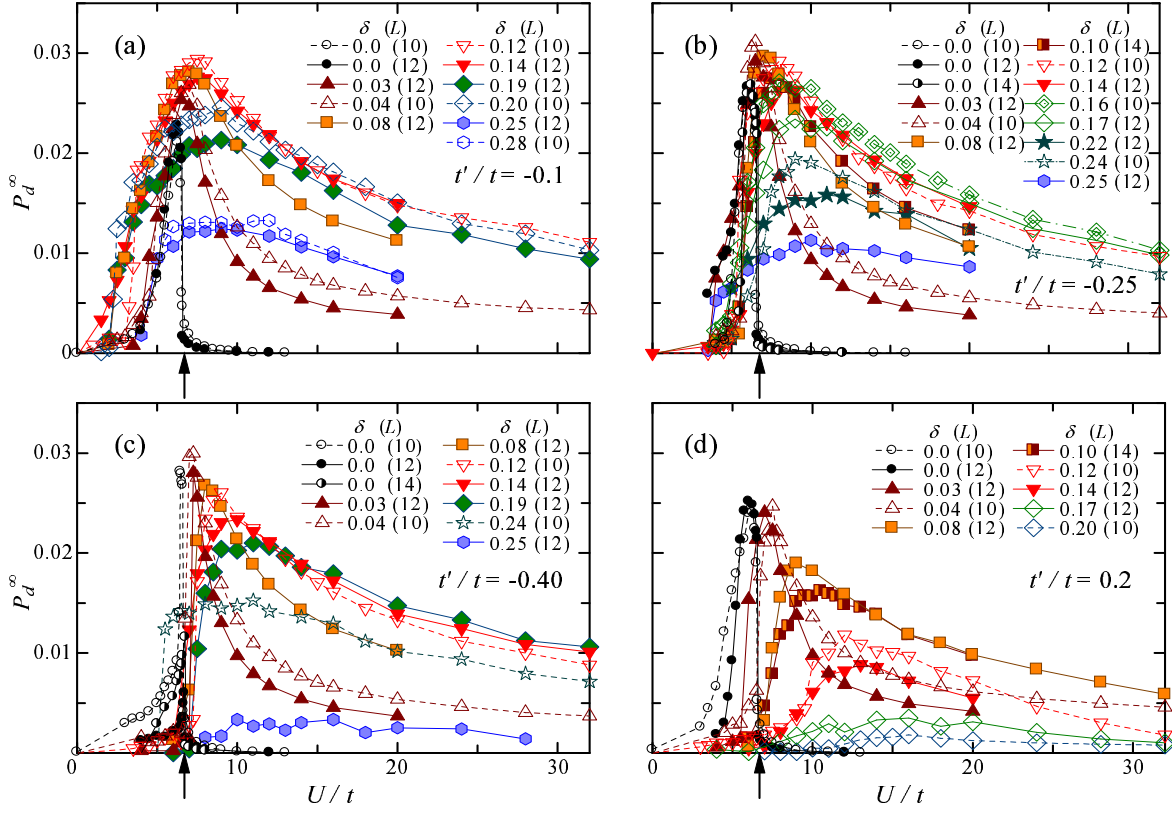


Fig. 24. (Color online) d -wave pairing correlation function as function of U/t for various values of doping rate δ (rounded off to two decimal places in legends). The values of t'/t are different among the four panels: (a)-(c) hole-doped and (d) electron-doped cases. Corresponding results for $t'/t = 0$ are given in Fig. 9. The arrow in each panel indicates the Mott transition point at half filling (circles).

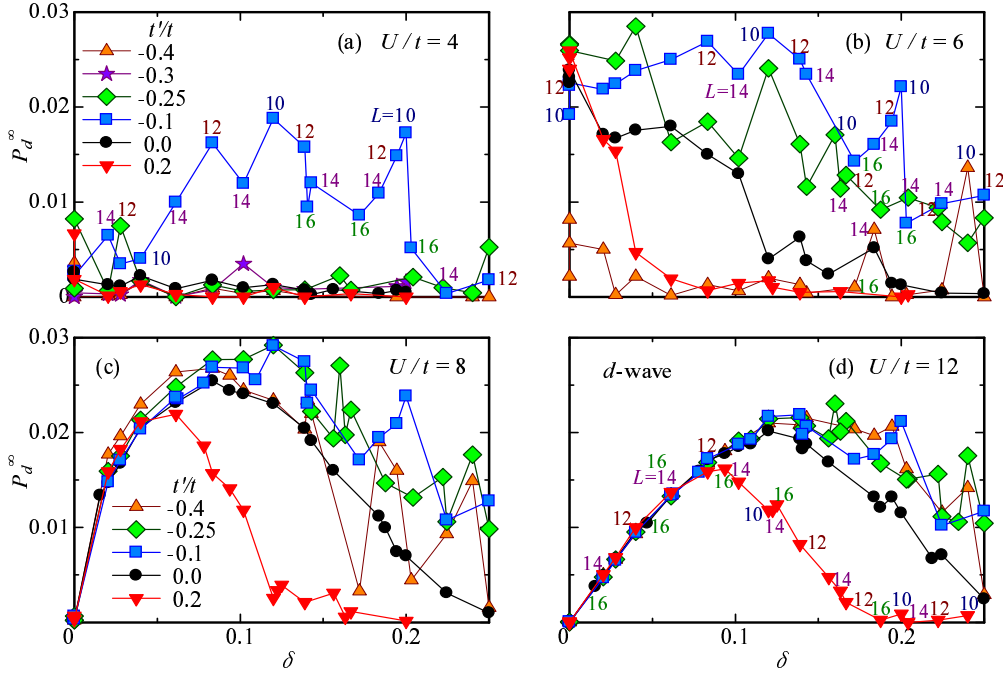


Fig. 25. (Color online) d -wave pairing correlation function as function of doping rate δ for various values of t'/t . The values of U/t are different among the four panels (a)-(d). The symbols indicating the values of t'/t are common to the four panels. Small digits beside some data points indicate the lattice size L ($= 10$ - 16) used.

and hole-doped cases [see also Fig. 28(c)]. At an optimum doping rate [Fig. 27(c)] the electron-hole asymme-

try stands out, and P_d^∞ decreases as t'/t increases in the electron-doped regime $t'/t > 0$ but P_d^∞ is steady and

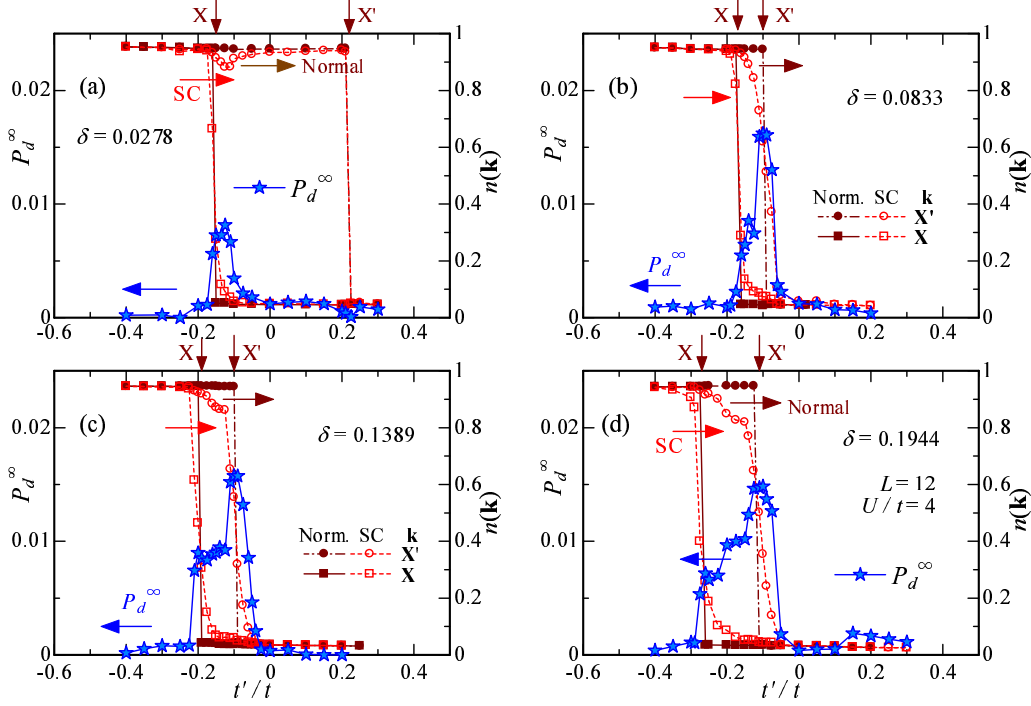


Fig. 26. (Color online) Correspondence between d -wave SC correlation function and jump in momentum distribution functions of Ψ_Q^F and Ψ_Q^d at two \mathbf{k} points ($\mathbf{k} = \mathbf{X}$ and \mathbf{X}') near $(\pi, 0)$, as t'/t varies, for a weak correlation ($U/t = 4$). The cases of four doping rates are shown for $L = 12$. The arrows on the upper axes indicate the values of t'/t at which the Fermi surfaces of Ψ_Q^F pass \mathbf{X} and \mathbf{X}' .

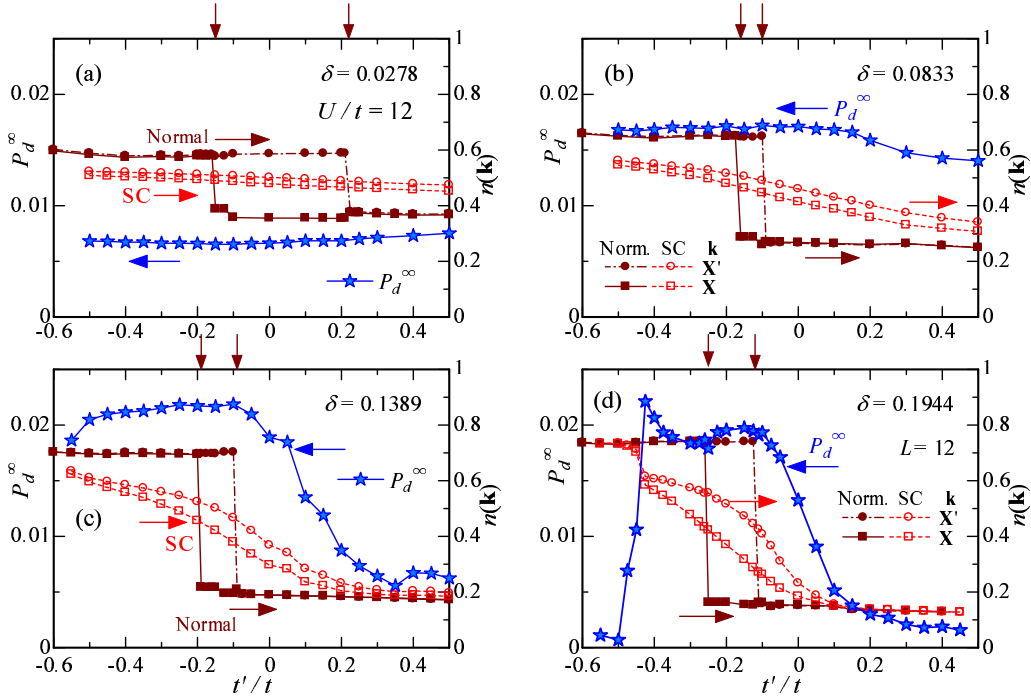


Fig. 27. (Color online) The same quantities as those in Fig. 26 are depicted in the same scales for a strong correlation ($U/t = 12$). The band renormalization by correlations is not considered here, but its effect seems irrelevant except near half filling.^{51, 88, 94, 124}

large throughout the range of $t'/t < 0$. This tendency is preserved for an overdoped regime [Fig. 27(d)], where P_d^∞ is still large in the range of hole-doped cuprates ($-0.4 \lesssim t'/t \lesssim -0.05$). On the other hand, the Fermi surface of Ψ_Q^F passes $\mathbf{k} = \mathbf{X}$ and \mathbf{X}' at the same t'/t as the weakly correlated cases, as indicated by arrows. For the

underdoped and optimally doped cases, P_d^∞ does not exhibit any special behavior at the positions of the arrows. Only in the overdoped case does P_d^∞ display a slight tendency of forming a shoulder near an arrow. Anyway, in the strongly correlated regime, the strength of SC is almost independent of the locus of the Fermi surface of the

underlying normal state, namely, the bare band structure, suggesting that P_d^∞ is determined by a mechanism qualitatively different from conventional BCS-type theories, which start from the instability of the Fermi surface of the normal state. We will return to this subject in §5.

To summarize the t'/t dependence of P_d^∞ , we show P_d^∞ for three different regimes of δ in Fig. 28. For a weak correlation ($U/t = 4$), the area of enhanced P_d^∞ is limited ($-0.25 \lesssim t'/t \lesssim -0.1$) regardless of δ , and the magnitude tends to vanish as L increases. For strongly correlated cases ($U/t \geq 8$), P_d^∞ is enhanced by moderate negative values of t'/t when δ is in the overdoped and optimally doped regimes. On the other hand, near half filling, the magnitude of P_d^∞ is steady, and tends to be independent of t'/t as U/t increases.

Finally, we point out that P_d^∞ becomes a weakly *increasing* function of t'/t near half filling and for very large U/t , as shown in Fig. 28(d). Such unexpected behavior was discovered for very slightly doped t - J models using the density matrix renormalization group¹²⁸ and exact diagonalization,¹²⁹ and seemed incompatible with the property of cuprates. Later, a VMC study⁵¹ based on the t - J model revealed that this feature is restricted to the close vicinity of half filling. The present result supports this finding and adds a requirement that the interaction should be considerably strong (e.g., $U/t = 16$).

5. Antinodal Electrons and Superconductivity

In §4.2, we argued that electrons near antinodal points are crucial for d -wave SC. In this section, we actually reveal a close relationship between the behavior of the momentum distribution function $n(\mathbf{k})$ near $\mathbf{k} = (\pi, 0)$ and the SC correlation function P_d^∞ in the strongly correlated regime.

First, let us recall again the t'/t dependence of P_d^∞ for sufficiently large values of U/t for comparison with that of $n(\mathbf{k})$. As discussed in ref. 17, the properties of Ψ_Q^d in the insulating phase ($U > U_c$ at half filling) are almost independent of t'/t . For small δ , the t'/t dependence of P_d^∞ is still weak as seen for $U/t = 12$ and 16 in Fig. 28(c), but for $\delta \gtrsim 0.1$, P_d^∞ comes to largely depend on t'/t , i.e., P_d^∞ tends to increase for $t'/t < 0$ and decrease for $t'/t > 0$ as shown in Figs. 28(b) and 28(a).

With this behavior of P_d^∞ in mind, we look at the t'/t dependence of $n(\mathbf{k})$ [eq. (26)]. In Fig. 29, $n(\mathbf{k})$ is plotted for six δ for $U/t = 12$. In each panel, data for various values of t'/t are displayed together. At half filling [Fig. 29(a)], $n(\mathbf{k})$ is almost independent of t'/t as mentioned, and does not have a discontinuity at any \mathbf{k} , because Ψ_Q^d is Mott insulating ($U_c/t \sim 6.5$ -7.2) with a charge density gap. Upon doping carriers, a discontinuity (Fermi surface) appears in the lattice-diagonal direction near $(\pi/2, \pi/2)$ [Figs. 29(b)-29(f)],¹⁰⁸ because Ψ_Q^d becomes SC with nodes of $\Delta_{\mathbf{k}}$ for $k_x = \pm k_y$ (and finally metallic). Meanwhile, it is in the antinodal area near $(\pi, 0)$, where the behavior of $n(\mathbf{k})$ markedly changes as t'/t varies; the degree of change culminates around the optimum doping rate ($\delta \sim 0.15$). Compared with that in the antinodal area, the change in $n(\mathbf{k})$ by t'/t is insignificant in other areas of \mathbf{k} . Thus, we became aware of a

and the electronic structure in the antinodal area.

In the overdoped regime ($\delta \gtrsim 0.2$), $n(\mathbf{k})$ exhibits a Fermi-liquid-like discontinuity (Fermi surface) in the antinodal area for some values of t'/t , i.e., on the segment $(0, 0)$ - $(\pi, 0)$ in the electron-doped cases ($t'/t > 0$), and on $(\pi, 0)$ - (π, π) for $t'/t \lesssim -0.4$ [Figs. 29(e) and 29(f)]. We find in Fig. 28(a) that when such a discontinuity appears, robust SC does not occur. Inversely, when $n(\mathbf{k})$ changes continuously and relatively slowly in the antinodal area [Figs. 29(b)-29(d)], P_d^∞ has a large and steady magnitude [Figs. 28(b) and 28(c)]. Such behavior appears in a broad range of t'/t , particularly in the underdoped regime. We will discuss this problem shortly.

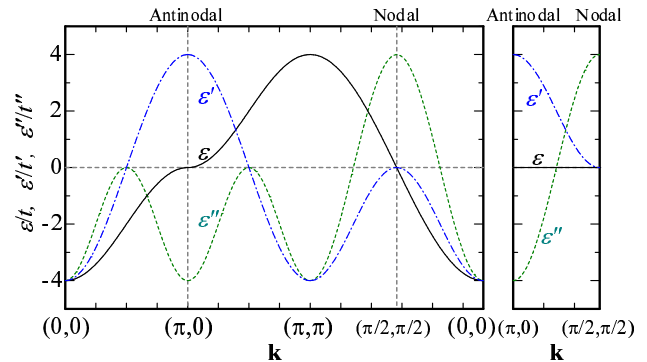


Fig. 30. (Color online) Elements of bare band dispersion relations along paths $(0, 0) \rightarrow (\pi, 0) \rightarrow (\pi, \pi) \rightarrow (0, 0)$ (left panel) and $(\pi, 0) \rightarrow (\pi/2, \pi/2) \rightarrow (0, 0)$ (right panel): $\varepsilon/t = -2(\cos k_x + \cos k_y)$, $\varepsilon'/t = -4 \cos k_x \cos k_y$, $\varepsilon''/t = -2(\cos 2k_x + \cos 2k_y)$. t'' indicates the hopping integral to the third-neighbor sites $(\pm 2, 0)$ and $(0, \pm 2)$, which is disregarded in this paper. The nodal $(\pi/2, \pi/2)$ and antinodal $(\pi, 0)$ points are marked by vertical dashed lines.

The above feature of $n(\mathbf{k})$ is more or less related to the band structure. In Fig. 30, the elements of the bare band dispersion relation $\varepsilon_{\mathbf{k}} [= \varepsilon + \varepsilon'(+\vare'')]$ are depicted. The dispersion of the pure square lattice ε ($t' = t'' = 0$) has a well-known flat part at $\varepsilon = 0$ around $(\pi, 0)$ (stationary in both k_x and k_y directions), where the Fermi surface passes for $\delta \sim 0$. The dispersion due to t' (ε') is also stationary but maximum at $(\pi, 0)$. Consequently, $\varepsilon_{\mathbf{k}}$ and the locus of the Fermi surface around $(\pi, 0)$ sensitively depend on t'/t . In contrast, at the $\varepsilon = 0$ point in the nodal direction $(\pi/2, \pi/2)$, ε' is zero and stationary, so that the change in $\varepsilon_{\mathbf{k}}$ by t'/t is small near $(\pi/2, \pi/2)$. Incidentally, the third-neighbor hopping t'' , which is omitted here but is often used as $t'' = -t'/2$ in the literature, works similarly to that of t' near $(\pi, 0)$ because $\varepsilon''/t'' \sim -\varepsilon'/t'$.¹³⁰

To relate the above feature of $n(\mathbf{k})$ to P_d^∞ quantitatively, we need a quantity that appropriately expresses this feature. The magnitude of $n(\mathbf{k})$ near $(\pi, 0)$ itself apparently does not represent the strength of SC. In fact, we found that the slope of $n(\mathbf{k})$,

$$|\nabla n(\mathbf{k})| = \sqrt{\left(\frac{\partial n(\mathbf{k})}{\partial k_x}\right)^2 + \left(\frac{\partial n(\mathbf{k})}{\partial k_y}\right)^2}, \quad (27)$$

around the antinodal point seems relevant.^{44, 124} The

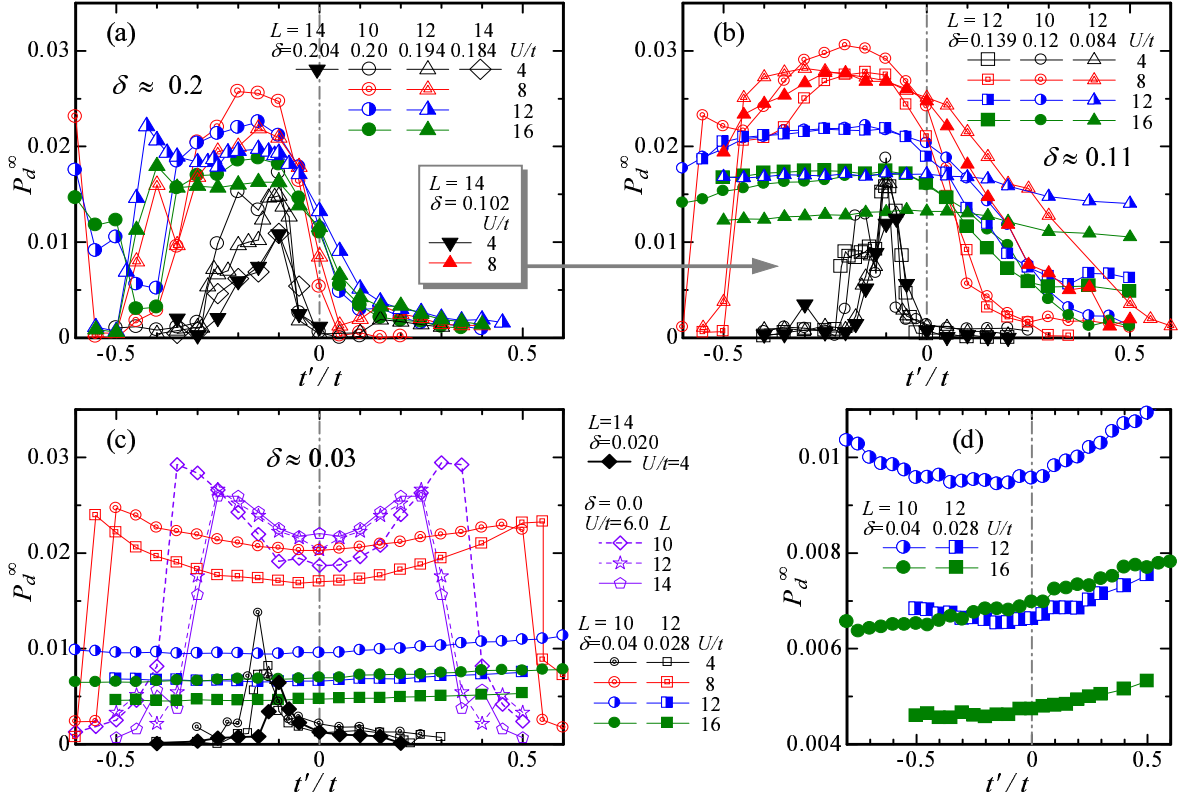


Fig. 28. (Color online) d -wave pairing correlation function as function of t'/t for several values of U/t . The doping rates δ are different among (a)-(c): (a) in the overdoped regime, $\delta \sim 0.20$, (b) in the optimally doped and underdoped regime, $\delta \sim 0.11$, and (c) nearly half filling $\delta \sim 0.03$. In (d), a magnification of (c) in the vertical axis is shown to emphasize the subtle variation in P_d^∞ .

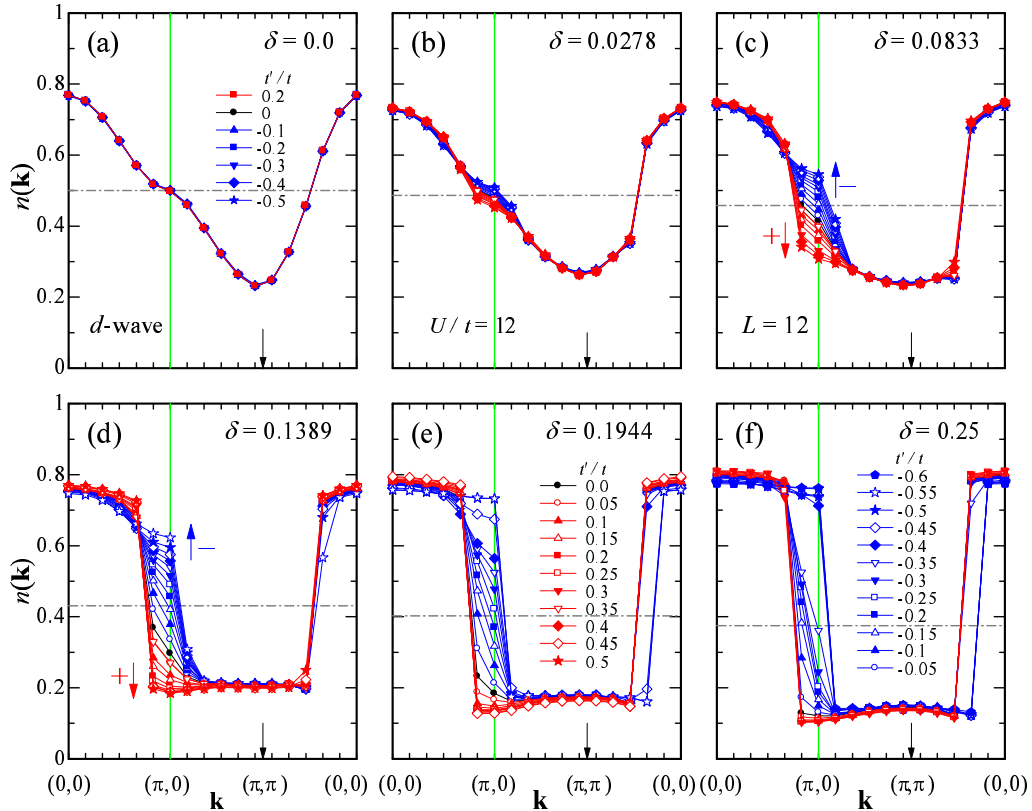


Fig. 29. (Color online) Momentum distribution function of d -wave state for various values of t'/t for $U/t = 12$ and $L = 12$; the behavior basically does not change even if U/t ($\gtrsim 10$) or L varies. The doping rates are different among the panels. The symbols for t'/t in (a), (e), and (f) are common to all panels. Owing to the boundary condition, k_y for each \mathbf{k} -point shifts by $\pi/(2L)$. The arrows with + [-] in (c) and (d) indicate the direction of variation for $t'/t > 0$ [$t'/t < 0$] when $|t'/t|$ increases; this t'/t dependence does not alter for (b), (e), and (f). The $(\pi, 0)$ point is marked with a vertical guide line, and the (π, π) point with a small arrow on the abscissa.

maximum of $|\nabla n(\mathbf{k})|$ is often used as an index of a quasi-Fermi surface and is reduced to a pure Fermi surface for $|\nabla n(\mathbf{k})| \rightarrow \infty$. Here, we estimate $|\nabla n(\mathbf{k})|$ near $\mathbf{k} = (\pi, 0)$ (abbreviated as $|\nabla n(\mathbf{X})|$) from the finite-size VMC data as follows: $\partial n(\mathbf{k})/\partial k_x$ and $\partial n(\mathbf{k})/\partial k_y$ are obtained from the finite differences of $n(\mathbf{k})$ between \mathbf{X}' and \mathbf{X} given in §4.3 and those between \mathbf{X} and $\mathbf{X}'' = \pi(1, \frac{2}{L})$, respectively.

In Fig. 31, we plot $n(\mathbf{k})$ for various δ ($L = 10-16$) for three values of t'/t at $U/t = 12$. In contrast to the t'/t dependence (Fig. 29), an appreciable variation exists at any \mathbf{k} , but the magnitude of variation in the antinodal area is still relatively large. We estimate $|\nabla n(\mathbf{X})|$ for each δ from Figs. 31(a)-31(c), and plot it as a function of δ with triangles in Figs. 31(d)-31(f), respectively, where the δ dependence of P_d^∞ is also displayed with circles. For $t' = 0$, the behavior of $|\nabla n(\mathbf{X})|$ is in close agreement with that of P_d^∞ except near half filling, where, however, the disagreement obviously stems from the system-size dependence.¹³¹ Thus, $|\nabla n(\mathbf{X})|$ is almost proportional to P_d^∞ for $t' = 0$. For $t'/t = 0.2$, the behavior of $|\nabla n(\mathbf{X})|$ is also nearly proportional to that of P_d^∞ ; $|\nabla n(\mathbf{X})|$ exhibits a similar system-size dependence near half filling. For $t'/t = -0.25$, the overall tendency of $|\nabla n(\mathbf{X})|$ coincides with that of P_d^∞ .

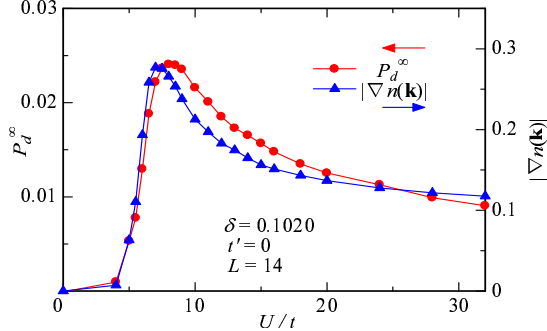


Fig. 32. (Color online) Comparison between SC correlation function P_d^∞ and $|\nabla n(\mathbf{k})|$ at $\mathbf{k} = \mathbf{X}' \sim (\pi, 0)$ as function of U/t for $t' = 0$ and $\delta = 0.102$. The scales of the two quantities are adjusted so as to roughly equalize the maximum magnitudes.

Finally, we touch on the U/t dependence of $|\nabla n(\mathbf{X})|$. If the simple d -wave BCS function without correlation factors is used, we have $|\nabla n(\pi, 0)| = 0$ by differentiating

$$n(\mathbf{k}) = |v_{\mathbf{k}}|^2 = \frac{1}{2} \left[1 - \frac{\varepsilon_{\mathbf{k}} - \zeta}{\sqrt{(\varepsilon_{\mathbf{k}} - \zeta)^2 + \Delta_{\mathbf{k}}^2}} \right], \quad (28)$$

so that finite $|\nabla n(\mathbf{X})|$ is considered as a correlation effect. Figure 32 shows a comparison of $|\nabla n(\mathbf{X})|$ and P_d^∞ of Ψ_Q^d for $t' = 0$ as a function of U/t in a slightly underdoped electron density. The two quantities are both almost zero for $U/t \lesssim 4$, and are in broad agreement for any U/t , suggesting that the electron distribution near $(\pi, 0)$ is important for d -wave SC irrespective of the correlation strength.

In this section, we have demonstrated that the

the antinodal point; this result confirms the discussions regarding the stability of the d -wave state in previous sections, and is consistent with recent experiments,^{32,93} which indicate that the antinodal electrons contribute to the SC gap. On the other hand, this result is contradictory to the concept of the dichotomy of electronic roles in the wave-number space, in which electrons near the nodal direction contribute to SC, and electrons near the antinodal point exclusively contribute to the pseudogaps.^{23,24} Similar results have recently been obtained by extended methods of DMFT.^{132,133}

6. Conclusions

With high- T_c cuprates in mind, we studied the U/t , δ , and t'/t dependences of the correlated $d_{x^2-y^2}$ -wave singlet state Ψ_Q^d and the AF state Ψ_Q^{AF} independently as doped Mott insulators, applying them to a 2D Hubbard (t - t' - U) model. The expectation values are calculated using a variational Monte Carlo method without additional approximations. The main results are recapitulated below.

(1) As U/t increases, Ψ_Q^d undergoes a sharp crossover of SC properties from a conventional BCS type to a kinetic-energy-driven type at $U = U_{\text{co}}$ somewhat larger than the bandwidth ($8t$). As δ decreases, U_{co} is continuously connected to the Mott transition point U_c at half filling. For $U < U_{\text{co}}$, SC, which is fragile, is enhanced by the pair scattering of the vector $\mathbf{Q} = (\pi, \pi)$ near the antinodes, according to the ordinary d -wave BCS theory. For $U/t \lesssim 5$, steady SC corresponding to that of high- T_c cuprates is not found. The SC correlation function P_d^∞ abruptly increases for $U/t \gtrsim 6$. Unconventional SC for $U > U_{\text{co}}$ is robust for wide ranges of t'/t and δ , which coincide with the ranges where the doublon-holon binding correlation—the essence of Mott physics—is effective, and the picture of the t - J model is valid. This SC cannot be explained by the instability of the Fermi surface in the underlying normal state.

(2) By comparing the δ dependence of the d -wave SC correlation function P_d^∞ with the dome shape of T_c and the condensation energy experimentally observed in cuprates, we showed that the effective value of U for cuprates must be larger than at least the Mott critical value U_c ($\sim 7t$). Furthermore, we found from the analysis of kinetic energy that there are two kinds of holons for $U > U_{\text{co}}$; a holon created during doublon formation does not contribute to conduction, but a holon introduced by doping becomes a carrier. Consequently, the number of doped holes (electrons) becomes equal to the number of carriers. This is a natural picture in the t - J model and consistent with various experimental results of cuprates.^{117,118} On the other hand, for $U < U_{\text{co}}$, all holons (electrons) work in the same manner as carriers, which make an ordinary large Fermi surface. This Fermi liquid feature is contradictory to that of cuprates.

(3) In view of the two-gap problem, the present result for $U > U_c$ is interpreted as follows: A gap for the singlet pair formation Δ_d , which possibly corresponds to a pseudogap, is a decreasing function of δ . Meanwhile, the strength of SC represented by P_d^∞ (related to the SC gap) is almost independent of δ .

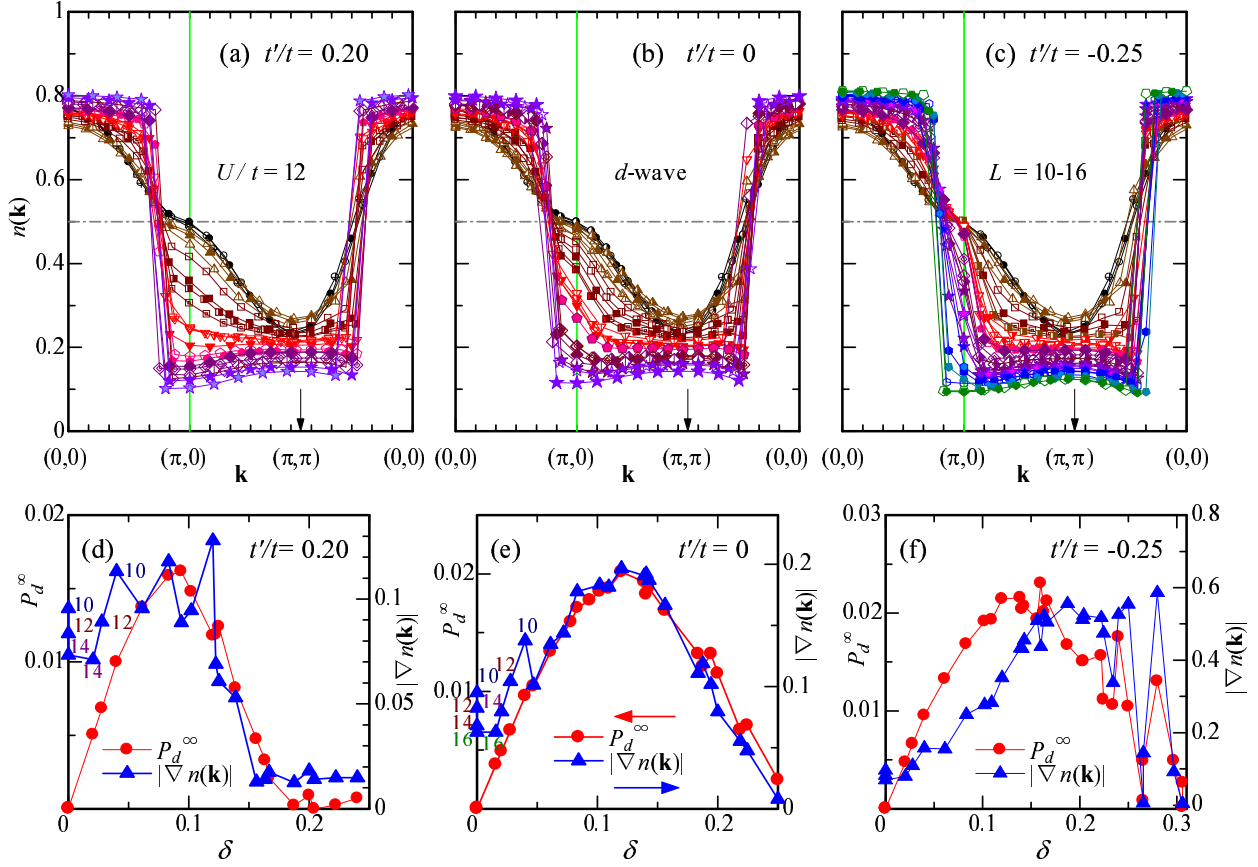


Fig. 31. (Color online) (a)-(c) Momentum distribution function of Ψ_Q^d for various values of δ at $U/t = 12$. The values of t'/t are different among the three panels. The data for $L = 10-16$ are simultaneously displayed. Detailed instructions for δ are omitted, but circles denote $\delta = 0$, upward triangles $\delta = 0.02-0.04$, squares $\delta = 0.06-0.11$, downward triangles $\delta = 0.12-0.14$, upward pentagons $\delta = 0.15-0.165$, diamonds $\delta = 0.165-0.21$, stars $\delta = 0.22-0.25$, hexagons $\delta = 0.26-0.29$, and downward pentagons $\delta = 0.29-0.31$. To adjust the scale in the section $(0,0)-(\pi,0)-(\pi,\pi)$, the locus of \mathbf{k} points between $(\pi,\pi)-(0,0)$ slightly shifts depending on L . (d)-(f) Comparison between SC correlation function P_d^∞ and $|\nabla n(\mathbf{k})|$ near $\mathbf{k} = (\pi,0)$ estimated from the data in (a)-(c) for the three values of t'/t . We adjust the scales of the two quantities so as to roughly equalize the maximum magnitudes. The small digits for $\delta \sim 0$ in (d) and (e) indicate the system size L used for the corresponding data point.

ten as the product of Δ_d and a factor indicating charge transportability such as the carrier density or the quasi-particle renormalization factor Z , which are increasing functions of δ for small δ . This suppression of charge fluctuation is imposed by the Mott physics. This feature of the SC gap is consistent with various theories based on the t - J model.

(4) A proper negative (positive) t'/t term stabilizes the SC (AF) state and destabilizes the AF (SC) state. A case of a very small δ and a quite large U/t is exceptional. Meanwhile, the AF state is intrinsically unstable in hole-doped cases ($t'/t \lesssim 0$), and the phase separates to the AF state with the local electron density $n = 1$ and to the SC state with $n < 0.85$.

(5) For the stability of AF state, the nesting of \mathbf{Q} is primarily important on the whole Fermi surface. On the other hand, crucial for SC is the pair scattering of \mathbf{Q} in the antinodal area, where the underlying band is flat. To check this aspect, we showed that the SC correlation P_d^∞ is closely connected to the slope of the momentum distribution function $|\nabla n(\mathbf{k})|$ near the antinodal point. This contradicts the often argued dichotomy of electronic roles in the \mathbf{k} space, i.e., electrons in the nodal (antinodal) area

exclusively contribute to SC (pseudogap).

Finally, we briefly mention some future problems. (i) It is important to include long-range hopping terms in the band dispersion and band renormalization effects owing to the electron correlation. (ii) We should check the coexistence of SC and AF orders and their mutual exclusion. (iii) In connection with the pseudogap problem, normal states with some symmetry breaking should be studied. (iv) Making the best use of the recent progress in VMC techniques,¹³⁴ we have to explore more precise trial wave functions.^{114,135} (v) We should study the role of doublons and holons in the SC phase in more detail, for instance, to confirm a recent proposal.¹³⁶

The authors thank Tsutomu Watanabe, Shun Tamura, and Takafumi Sato for useful discussions. This work is partly supported by Grants-in-Aid from the Ministry of Education, Culture, Sports, Science and Technology.

Appendix A: Hubbard model for cuprates

To consider CuO_2 planes, an appropriate starting model is the d - p model composed of O- $2p$ and Cu- $3d_{x^2-y^2}$ orbitals. The d - p model is reducible to simpler models that still capture the essence of CuO_2 planes. Since a

Table B.1. Absolute values of total energy of the d -wave state, $|E/t|$, are compared among the three D-H correlation factors for $\delta > 0$, $t'/t = 0$, and $L = 10$. The last digits may have some errors.

δ	0.20			0.12		
U/t	\mathcal{P}_Q^D	\mathcal{P}_Q^S	\mathcal{P}_Q^{DH}	\mathcal{P}_Q^D	\mathcal{P}_Q^S	\mathcal{P}_Q^{DH}
4	1.0754	1.0773	1.0773	0.9914	0.9935	0.9935
6	0.9237	0.9282	0.9284	0.7979	0.8035	0.8038
8	0.8216	0.8288	0.8291	0.6750	0.6841	0.6854
10	0.7545	0.7626	0.7634	0.6010	0.6094	0.6121
12	0.7084	0.7165	0.7177	0.5518	0.5583	0.5624
16	0.6502	0.6576	0.6591	0.4903	0.4936	0.4988

reduced to a Hubbard model on a square lattice by eliminating the degree of freedom for the O- $2p$ orbitals. In contrast, a doped hole enters an O- $2p$ orbital; a Zhang-Rice singlet is formed, through which the model for a low dopant density is reduced to the t - J model on a square lattice with small J/t .² This t - J model is connected to the Hubbard model with large U/t ($= 4t/J$) through the strong-coupling expansion¹³⁷ within the approximation of neglecting the pair-hopping (three-site) terms. Thus, the Hubbard model on a square lattice is derived as an effective model for both electron-doped (ED) and hole-doped (HD) cuprates. Note, however, that the effective value of U/t in the Hubbard model may differ between ED and HD cases owing to the distinct derivation paths, even if the actual values of U in the Cu- $3d_{x^2-y^2}$ orbitals are identical between the two.

Another vital element of the model, eq. (1), is that one can map a more-than-half-filled case ($n > 1$) to a less-than-half-filled case ($n < 1$) by taking advantage of the antisymmetric level structure with respect to $n = 1$. The band dispersion, eq. (2), for $\tilde{\mathbf{k}} = (\pi - k_y, \pi - k_x)$, which is the symmetric point of \mathbf{k} with respect to the Fermi surface at half filling for $t' = 0$ (AF Brillouin zone boundary), is written as

$$\tilde{\varepsilon}(\tilde{\mathbf{k}}) = 2\tilde{t}(\cos k_x + \cos k_y) - 4\tilde{t}' \cos k_x \cos k_y, \quad (\text{A}\cdot 1)$$

where tildes are the marks for $\tilde{\mathbf{k}}$. To satisfy $\varepsilon(\mathbf{k}) = -\tilde{\varepsilon}(\tilde{\mathbf{k}})$, we need the relations $\tilde{t} = t$ and $\tilde{t}' = -t'$, which are represented by a canonical (electron-hole) transformation,

$$c_{i\sigma}^\dagger \rightarrow e^{i\mathbf{Q}\cdot\mathbf{r}_i} \tilde{c}_{i\sigma}, \quad (\text{A}\cdot 2)$$

with $\mathbf{Q} = (\pi, \pi)$. Under this transformation, the model, eq. (1), is invariant except for the addition of a constant $U(N_s - N)$. Consequently, calculations for an ED system with electron density $n = 1 + \delta$ ($\delta > 0$) and t'/t (< 0) can be replaced by those for the less-than-half-filled case with $1 - \delta$ and $|t'/t|$, if we consider that t'/t is negative for both ED and HD cuprates.

Appendix B: Details of doublon-holon factors

In this Appendix, we compare different forms of the D-H correlation factor \mathcal{P}_Q [eq. (5)] to show that the difference in results among Q_j^D [eq. (7)] and other forms of Q_j is insignificant. Here, \mathcal{P}_Q between nearest-neighbor sites is mainly considered, because \mathcal{P}_Q between further sites only makes a minor difference.²⁰

At half filling, symmetric projections such as \mathcal{P}_Q with

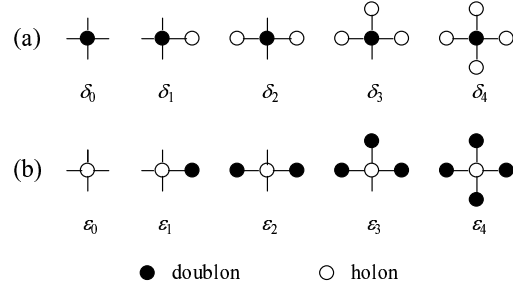


Fig. B.1. (a) Local configurations around a doublon are classified according to the number of holons in the nearest-neighbor sites. (b) A similar classification around a holon.

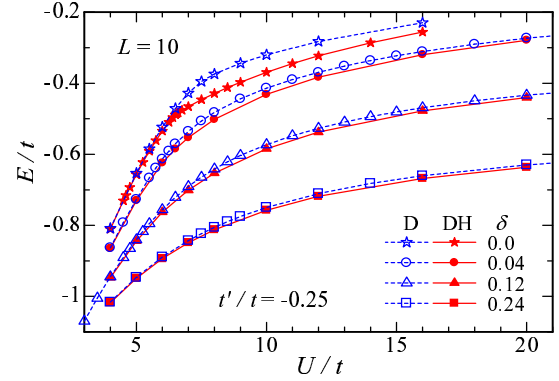


Fig. B.2. (Color online) The total energy of Ψ_j^d with \mathcal{P}_j^{DH} (solid symbols) is compared with that with \mathcal{P}_j^D (open symbols) as a function of U/t for four δ . At half filling, Q_j^{DH} is reduced to Q_j^S (solid stars).¹⁷ The tendency for other values of t'/t is similar.

the particle-hole or doublon-holon symmetry. For $\delta > 0$, however, this symmetry is broken, and the number of holons always exceeds that of doublons. Consequently, if \mathcal{P}_j^S is used, the configurations δ_2 , δ_3 , and δ_4 illustrated in Fig. B.1 seem to appear frequently as δ increases. In fact, a recent study¹²⁴ using a detailed parameterization for Q_j has revealed that such configurations rarely appear for large U/t , because they increase the interaction energy Ud . Anyway, we consider another asymmetric form of Q_j , which is a natural extension of Q_j^S :

$$Q_j^{DH} = \mu_d d_j \prod_{\tau} (1 - h_{j+\tau}) + \mu_h h_j \prod_{\tau} (1 - d_{j+\tau}), \quad (\text{B}\cdot 1)$$

where binding parameters for holons μ_h and doublons μ_d are optimized independently. At half filling, Q_j^{DH} is reduced to Q_j^S ($\mu_h = \mu_d$) to retrieve the symmetry. As δ increases, μ_h is expected to decrease much faster than μ_d because ε_2 comes to appear less frequently than δ_2 ; therefore Q_j^{DH} approaches Q_j^D (μ_h rapidly decreases). As shown in Table B.1,¹³⁹ the variational energy of Q_j^{DH} is improved compared with that of Q_j^S , especially for large U/t . In the following, we compare the asymmetric forms Q_j^{DH} and Q_j^D .

In Fig. B.2, the total energies of the d -wave state are compared between Q_j^D and Q_j^{DH} for $t'/t = -0.25$. In Table B.2, we list the energy improvements by Q_j^{DH} com-

Table B.2. Improvements in total energy by Ψ_Q^{DH} on Ψ_Q^{D} as percentages, $(E^{\text{D}} - E^{\text{DH}})/|E^{\text{D}}| \times 100$, for various parameter values and $L = 10$, which satisfy the closed-shell condition.

t'/t	-0.25				0			
δ	0.24	0.12	0.04	0.0	0.20	0.12	0.04	0.0
U/t								
4	0.2	0.2	0.2	0.2	0.2	0.2	0.2	0.3
6	0.5	1.0	1.8	2.0	0.5	0.7	1.5	1.9
8	0.8	1.8	4.1	14.6	0.9	1.5	3.9	14.0
10	1.0	2.0	4.2	15.3	1.2	1.8	4.0	15.0
12	1.1	2.0	3.7	14.3	1.3	1.9	3.7	14.0
16	1.2	1.8	2.8	11.4	1.4	1.7	2.7	11.3

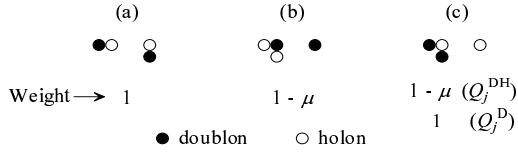


Fig. B.3. Weight assignment by Q_j^{DH} and by Q_j^{D} to local configurations with two doublons and two holons typical for $U \sim U_{\text{co}}$ at half filling. All the sites in the background are singly occupied. In each case, only relative positions of doublons to holons are illustrated. In (a), there are two δ_1 and two ε_1 ; in (b), δ_2 , δ_0 , and two ε_1 ; and in (c), ε_2 , ε_0 , and two δ_1 .

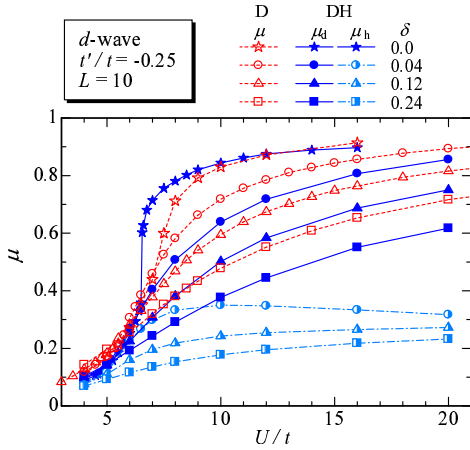


Fig. B.4. (Color online) Comparison of optimized D-H correlation parameters between Q_j^{D} (μ) and Q_j^{DH} (μ_d and μ_h) for nearest-neighbor sites.

pared with Q_j^{D} ($\Delta E = E^{\text{D}} - E^{\text{DH}}$) for some values of δ and t'/t as functions of U/t . In every case, the energy is improved for Q_j^{DH} . Comparing $\Delta E/t$ for $t'/t = -0.25$ and 0, we find that ΔE only slightly depends on t'/t . For each δ , $\Delta E/t$ is maximum near $U_{\text{co}}/t = 10$, especially at half filling, and Q_j^{DH} ($=Q_j^{\text{S}}$) becomes highly advantageous for $U > U_c$. For a fixed U/t , $\Delta E/t$ decreases as δ increases.

We briefly consider the reason why Q_j^{DH} is advantageous at half filling and for $U \sim U_{\text{co}}$. Assume that only two doublons and two holons exist in a local electron configuration at half filling; typical ones frequently appearing for $U \sim U_{\text{co}}$ are shown in Fig. B.3. The Gutzwiller factor assigns a common weight g^2 to each of these configurations. Regarding the D-H factors, $\mathcal{P}_Q^{\text{DH}}$ and \mathcal{P}_Q^{D} give

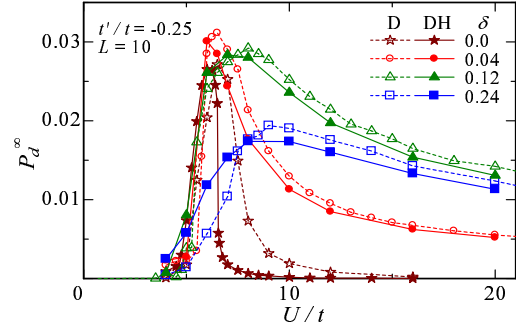


Fig. B.5. (Color online) Comparison of d -wave pair correlation function between two D-H correlation factors, $\mathcal{P}_Q^{\text{DH}}$ and \mathcal{P}_Q^{D} . The behavior of P_d^∞ is similar for other values of t'/t .

the same weights of 1 and $1 - \mu$ for the configurations (a) and (b), respectively;¹²⁴ however, for an unfavorable configuration (c), \mathcal{P}_Q^{D} gives 1, but $\mathcal{P}_Q^{\text{DH}}$ reduces the weight as $1 - \mu$. Thus, Q_j^{DH} becomes better than Q_j^{D} at $\delta = 0$ and for $U \sim U_{\text{co}}$. When holes are doped, configurations such as ε_2 (also ε_3 and ε_4) appearing in Fig. B.3(c) are rapidly suppressed; accordingly, the difference between Q_j^{DH} and Q_j^{D} narrows. This aspect is clearly seen in the optimized D-H binding factors μ in Q_j^{D} and μ_d and μ_h in Q_j^{DH} , as shown in Fig. B.4. As δ increases, μ_d becomes slightly smaller, but μ_h considerably and rapidly decreases compared with μ in Q_j^{D} denoted by open symbols.

Because the optimized values of the other variational parameters are similar between the two cases of $\mathcal{P}_Q^{\text{DH}}$ and \mathcal{P}_Q^{D} (not shown), physical quantities, e.g., $n(\mathbf{k})$, $S(\mathbf{q})$, and $N(\mathbf{q})$, thereof become similar (not shown). Among them, the d -wave pairing correlation function exhibits a relatively large difference, as shown in Fig. B-5; the maximum P_d^∞ is located at a slightly smaller U/t for Q_j^{DH} . However, the difference remains quantitative.

In conclusion, the D-H correlation factor \mathcal{P}_Q^{D} possesses properties sufficiently close to those of an improved factor $\mathcal{P}_Q^{\text{DH}}$ at least for $\delta > 0$.

Appendix C: Pairing correlation function

We explain the details of how we determine long-distance values (P_d^∞) of the $d_{x^2-y^2}$ -wave SC correlation function $P_d(\mathbf{r})$ defined by eq. (20) with eq. (21), to avoid misunderstanding. If $P_d(\mathbf{r})$ remains finite for $|\mathbf{r}| \rightarrow \infty$, an off-diagonal long-range order exists. For finite systems, however, one must be careful in estimating $P_d(\mathbf{r})$ for $|\mathbf{r}| = \infty$.

In Fig. C-1, the behavior of $P_d(\mathbf{r})$ for the noninteracting case ($U/t = 0$) is compared among different system sizes. Here, the path of \mathbf{r} is chosen as shown in Fig. C-2(c). Because SC does not occur for $U/t = 0$, $P_d(\mathbf{r})$ must vanish for large $|\mathbf{r}|$. However, for small systems such as $L = 10$ and 12, $P_d(\mathbf{r})$ still has an appreciable magnitude at distant points, e.g., $\mathbf{r} = (L/2, 0)$ and $\mathbf{r} = (L/2, L/2)$. Furthermore, the location of a large magnitude of $P_d(\mathbf{r})$ depends on t'/t and δ . If we require that $P_d(\mathbf{r})$ should vanish for every distant point in this scale, we need to use a system with $L \gtrsim 30$. Such a system is not feasible for the present study of U/t .

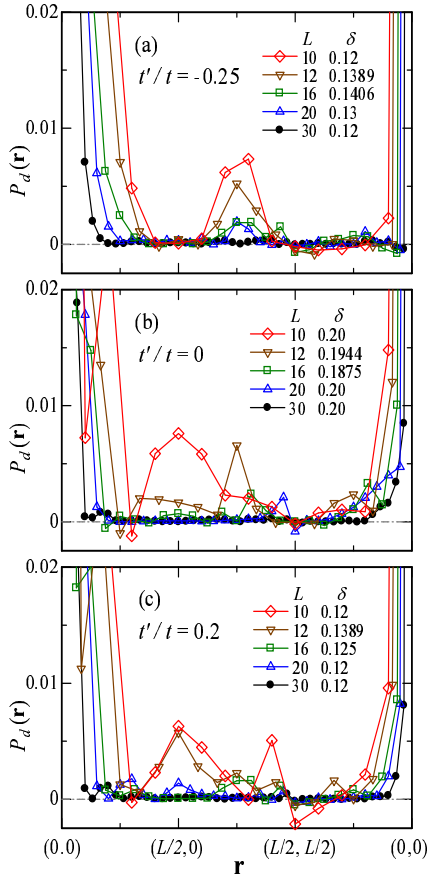


Fig. C.1. (Color online) System-size dependence of d -wave SC correlation function $P_d(\mathbf{r})$ for noninteracting systems ($U/t = 0$). The path of \mathbf{r} is shown in Fig. C.2(c). The values of t'/t and δ are (a) -0.25 and ~ 0.13 , (b) 0 and ~ 0.20 , and (c) 0.2 and ~ 0.13 , respectively. δ is chosen so as to satisfy the closed-shell condition under the same boundary condition as that in the VMC calculations. The data are obtained using the analytic formula.

as shown in Fig. C.2. Fortunately, we found that $|P_d(\mathbf{r})|$ for $\mathbf{r} = (L/2 - 1, L/2) \equiv \mathbf{r}_\infty$, which is next to the furthestmost point, is substantially zero (less than 10^{-4}) at $U = 0$ regardless of t'/t , δ , and L , and remains smaller than those for $\mathbf{r} \neq \mathbf{r}_\infty$ for small U/t . Hence, we employ $P_d(\mathbf{r}_\infty)$ as P_d^∞ for small U/t ($0 \leq U \leq U_{\max}$), where U_{\max} indicates the U of the largest $P_d(\mathbf{r})$ for a fixed t'/t . Thereby, the artificial increase in $P_d(\mathbf{r})$ owing to the finite sizes can be eliminated.

For large U/t ($U > U_{\max}$), P_d^∞ can be determined more confidently. The U/t dependence of $P_d(\mathbf{r})$ for fixed L and δ is shown in Fig. C.2. $P_d(\mathbf{r})$ exhibits finite-size fluctuations for $U \lesssim U_{\max}$, but becomes almost constant for $|\mathbf{r}| \geq 3^{140}$ regardless of t'/t and L for $U \gtrsim U_{\max}$. This behavior is the same as that found for the t - J model,⁵¹ and reflects the short-range nature of strong correlation. Thus, we use the average $P_d(\mathbf{r})$ for $|\mathbf{r}| \geq 3$ as P_d^∞ for $U > U_{\max}$.

In summary, as a suitable indicator of the d -wave SC order, we safely define the long-distance value of $P_d(\mathbf{r})$

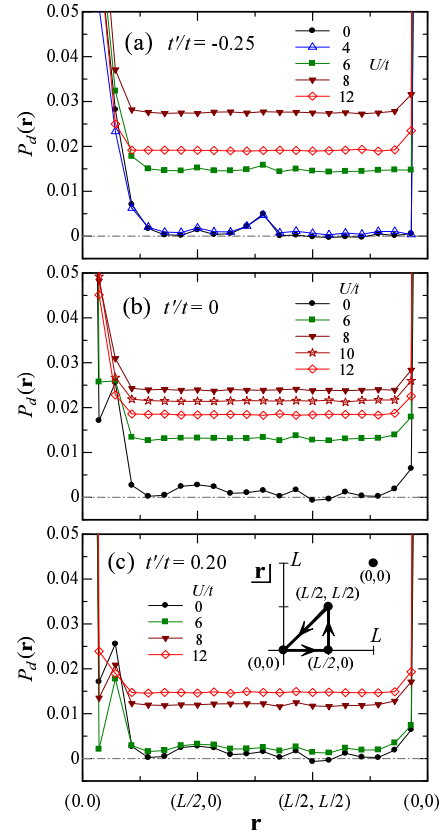


Fig. C.2. (Color online) U/t dependence of d -wave SC correlation function $P_d(\mathbf{r})$ for $L = 14$ and $\delta = 0.102$. The path of \mathbf{r} is depicted in (c); \mathbf{r}_∞ is not on this path. The values of t'/t are (a) -0.25 (hole doped), (b) 0 , and (c) 0.2 (electron doped). In these systems, $U_{\max}/t = 8.0$, 8.1 , and 10.5 for $t'/t = -0.25$, 0 , and 0.2 , respectively. In each case, the closed-shell condition is satisfied. Note that the scale of the vertical axis is larger than that in Fig. C.1. The data are obtained using the analytic formula for $U/t = 0$ and VMC otherwise.

for finite systems by

$$P_d^\infty = \begin{cases} P_d(\mathbf{r}_\infty) & (U < U_{\max}) \\ \frac{1}{M} \sum_{|\mathbf{r}_j| \geq 3} P_d(\mathbf{r}_j) & (U \geq U_{\max}) \end{cases}, \quad (\text{C.1})$$

where $\mathbf{r}_\infty = (L/2 - 1, L/2)$ and M is the number of vectors \mathbf{r}_j satisfying $|\mathbf{r}_j| \geq 3$.

- 1) P. W. Anderson: Science **235** (1987) 1196.
- 2) F. C. Zhang and T. M. Rice: Phys. Rev. B **37** (1988) 3759.
- 3) For instance, D. J. Scalapino: Phys. Rep. **250** (1995) 329; P. W. Anderson, P. A. Lee, M. Randeria, T. M. Rice, N. Trivedi, and F. C. Zhang: J. Phys. Cond. Mat. **16** (2004) R755.
- 4) P. A. Lee, N. Nagaosa, and X.-G. Wen: Rev. Mod. Phys. **78** (2006) 17.
- 5) M. Ogata and H. Fukuyama: Rep. Prog. Phys. **71** (2008) 036501.
- 6) For instance, T. Moriya and K. Ueda: Adv. Phys. **49** (2000) 555; Y. Yanase, T. Jujo, T. Nomura, H. Ikeda, T. Hotta, and K. Yamada: Phys. Rep. **387** (2003) 1; H. Kontani, K. Kanki, and K. Ueda: Phys. Rev. B **59** (1999) 14723.
- 7) C. J. Halboth and W. Metzner: Phys. Rev. B **61** (2000) 7364;

- D. Zanchi and H.J. Schulz: Phys. Rev. B **61** (2000) 13609; N. Furukawa, T.M. Rice, and N. Salmhofer: Phys. Rev. Lett. **81** (1998) 3195.
- 8) A. Moreo: Phys. Rev. B **45** (1992) 5059; N. Furukawa and M. Imada: J. Phys. Soc. Jpn. **61** (1992) 3331; K. Kuroki and H. Aoki: Phys. Rev. B **56** (1997) R14287; M. Guerrero, G. Ortiz, and J. E. Gubernatis: Phys. Rev. B **59** (1999) 1706.
 - 9) T. Aimi and M. Imada: J. Phys. Soc. Jpn. **76** (2007) 113708.
 - 10) T. Yanagisawa: J. Phys. Soc. Jpn. **79** (2010) 063708.
 - 11) W. L. Millman: Phys. Rev. **138** (1965) A442.
 - 12) D. Ceperley, G. V. Chester, and K. H. Kalos: Phys. Rev. B **16** (1977) 3081.
 - 13) H. Yokoyama and H. Shiba: J. Phys. Soc. Jpn. **57** (1988) 2482.
 - 14) C. Gros: Ann. Phys. (New York) **189** (1989) 53.
 - 15) H. Yokoyama and M. Ogata: J. Phys. Soc. Jpn. **65** (1996) 3615.
 - 16) H. Yokoyama, Y. Tanaka, M. Ogata, and H. Tsuchiura: J. Phys. Soc. Jpn. **73** (2004) 1119.
 - 17) H. Yokoyama, M. Ogata, and Y. Tanaka: J. Phys. Soc. Jpn. **75** (2006) 114706.
 - 18) M. Ogata, H. Yokoyama, Y. Yanase, Y. Tanaka, and H. Tsuchiura: J. Phys. Chem. Solids **67** (2006) 37.
 - 19) H. Yokoyama, Y. Tanaka, and M. Ogata: J. Phys. Chem. Solids **67** (2006) 47.
 - 20) T. Miyagawa and H. Yokoyama: J. Phys. Soc. Jpn. **80** (2011) 084705, and Physica C **471** (2011) 738.
 - 21) H. Yokoyama, T. Miyagawa, and M. Ogata: J. Phys. Soc. Jpn. **80** (2011) 084607, and Physica C **471** (2011) 730.
 - 22) M. Imada, A. Fujimori, and Y. Tokura: Rev. Mod. Phys. **70** (1998) 1039.
 - 23) For instance, G. Deutscher: Nature **397** (1999) 410; A. J. Millis: Science **314** (2006) 1888; S. Hüfner, M. A. Hossain, A. Damascelli, and G. A. Sawatzky: Rep. Prog. Phys. **71** (2008) 062501.
 - 24) T. Yoshida, M. Hashimoto, I. M. Vishik, Z.-X. Shen, and A. Fujimori: J. Phys. Soc. Jpn. **81** (2012) 011006.
 - 25) M. Le Tacon, A. Sacuto, A. Georges, G. Kotliar, Y. Gallais, D. Colson, and A. Forget: Nat. Phys. **2** (2006) 537.
 - 26) K. Tanaka, W. S. Lee, D. H. Lu, A. Fujimori, T. Fujii, Risdiana, I. Terasaki, D. J. Scalapino, T. P. Devereaux, Z. Hussain, and Z.-X. Shen: Science **314** (2006) 1910; T. Kondo, T. Takeuchi, A. Kaminski, S. Tsuda, and S. Shin: Phys. Rev. Lett. **98** (2007) 267004.
 - 27) M. Hashimoto, T. Yoshida, K. Tanaka, A. Fujimori, M. Okusawa, S. Wakimoto, K. Yamada, T. Kakeshita, H. Eisaki, and S. Uchida: Phys. Rev. B **75** (2007) 140503.
 - 28) M. C. Boyer, W. D. Wise, K. Chatterjee, M. Yi, T. Kondo, T. Takeuchi, H. Ikuta, and E. W. Hudson: Nat. Phys. **3** (2007) 802.
 - 29) Y. Wang, L. Li, and N. P. Ong: Phys. Rev. B **73** (2006) 024510.
 - 30) A. Kanigel, M. R. Norman, M. Randeria, U. Chatterjee, S. Souma, A. Kaminski, H. M. Fretwell, S. Rosenkranz, M. Shi, T. Sato, T. Takahashi, Z. Z. Li, H. Raffy, K. Kadowaki, D. Hinks, L. Ozyuzer, and J. C. Campuzano: Nat. Phys. **2** (2006) 447.
 - 31) T. Valla, A. V. Fedorov, J. Lee, J. C. Davis, and G. D. Gu: Science **314** (2006) 1914.
 - 32) K. Terashima, H. Matsui, T. Sato, T. Takahashi, M. Kofu, and K. Hirota: Phys. Rev. Lett. **99** (2007) 017003; M. Shi, J. Chang, S. Pailh s, M. R. Norman, J. C. Campuzano, M. Mansson, T. Claesson, O. Tjernberg, A. Bendounan, L. Patthey, N. Momono, M. Oda, M. Ido, C. Mudry, and J. Mesot: Phys. Rev. Lett. **101** (2008) 047002; M. Shi, A. Bendounan, E. Razzoli, S. Rosenkranz, M. R. Norman, J. C. Campuzano, J. Chang, M. Mansson, Y. Sassa, T. Claesson, O. Tjernberg, L. Patthey, N. Momono, M. Oda, M. Ido, S. Guerrero, C. Mudry, and J. Mesot: Europhys. Lett. **88** (2009) 27008.
 - 33) J.-H. Ma, Z.-H. Pan, F. C. Niستمسكي, M. Neupane, Y.-M. Xu, P. Richard, K. Nakayama, T. Sato, T. Takahashi, H.-Q. Luo, L. Fang, H.-H. Wen, Z. Wang, H. Ding, and V. Madhavan:
 - 34) T. Yoshida, M. Hashimoto, S. Ideta, A. Fujimori, K. Tanaka, N. Mannella, Z. Hussain, Z.-X. Shen, M. Kubota, K. Ono, S. Komiya, Y. Ando, H. Eisaki, and S. Uchida: Phys. Rev. Lett. **103** (2009) 037004.
 - 35) K. Nakayama, T. Sato, Y.-M. Xu, Z.-H. Pan, P. Richard, H. Ding, H.-H. Wen, K. Kudo, T. Sasaki, N. Kobayashi, and T. Takahashi: Phys. Rev. B **83** (2011) 224509.
 - 36) L. Yu, D. Munzar, A. V. Boris, P. Yordanov, J. Chaloupka, Th. Wolf, C. T. Lin, B. Keimer, and C. Bernhard: Phys. Rev. Lett. **100** (2008) 177004.
 - 37) A. Dubroka, M. R ssle, K. W. Kim, V. K. Malik, D. Munzar, D. N. Basov, A. A. Schafgans, S. J. Moon, C. T. Lin, D. Haug, V. Hinkov, B. Keimer, Th. Wolf, J. G. Storey, J. L. Tallon, and C. Bernhard: Phys. Rev. Lett. **106** (2011) 047006.
 - 38) R. Daou, J. Chang, D. LeBoeuf, O. Cyr-Choini re, F. Lalibert , N. Doiron-Leyraud, B. J. Ramshaw, R. Liang, D. A. Bonn, W. N. Hardy, and L. Taillefer: Nature **463** (2010) 519.
 - 39) M. J. Lawler, K. Fujita, J. Lee, A. R. Schmidt, Y. Kohsaka, C. K. Kim, H. Eisaki, S. Uchida, J. C. Davis, J. P. Sethna, and E.-A. Kim: Nature **466** (2010) 347; A. Mesaros, K. Fujita, H. Eisaki, S. Uchida, J. C. Davis, S. Sachdev, J. Zaanen, M. J. Lawler, and E.-A. Kim: Science **333** (2011) 426.
 - 40) K. K. Gomes, A. N. Pasupathy, A. Pushp, S. Ono, Y. Ando, and A. Yazdani: Nature **447** (2007) 569.
 - 41) Y. Kohsaka, T. Hanaguri, M. Azuma, M. Takano, J. C. Davis, and H. Takagi: Nat. Phys. **8** (2012) 534.
 - 42) K. Fujita, A. R. Schmidt, E.-A. Kim, M. J. Lawler, D. H. Lee, J. C. Davis, H. Eisaki, and S. Uchida: J. Phys. Soc. Jpn. **81** (2012) 011005.
 - 43) H. -B. Yang, J. D. Rameau, P. D. Johnson, T. Valla, A. Tsvelik, and G. D. Gu: Nature **456** (2008) 77.
 - 44) H. Yokoyama, M. Ogata, and K. Kobayashi: Physica C **470** (2010) S149.
 - 45) H. Yokoyama, S. Tamura, T. Miyagawa, K. Kobayashi, and M. Ogata: Phys. Proc. **27** (2012) 60.
 - 46) T. Tanamoto, H. Kohno, and H. Fukuyama: J. Phys. Soc. Jpn. **61** (1992) 1886.
 - 47) T. Tohyama and S. Maekawa: Phys. Rev. B **49** (1994) 3596; T. Tohyama: Phys. Rev. B **70** (2004) 174517.
 - 48) R. J. Gooding, K. J. E. Vos, and P. W. Leung: Phys. Rev. B **50** (1994) 12866.
 - 49) R. Raimondi, J. H. Jefferson, and L. F. Feiner: Phys. Rev. B **53** (1996) 8774.
 - 50) E. Pavarini, I. Dasgupta, T. Saha-Dasgupta, O. Jepsen, and O. K. Andersen: Phys. Rev. Lett. **87** (2001) 047003.
 - 51) C. T. Shih, T. K. Lee, R. Eder, C.-Y. Mou, and Y. C. Chen: Phys. Rev. Lett. **92** (2004) 227002.
 - 52) K. Tanaka, T. Yoshida, A. Fujimori, D. H. Lu, Z.-X. Shen, X.-J. Zhou, H. Eisaki, Z. Hussain, S. Uchida, Y. Aiura, K. Ono, T. Sugaya, T. Mizuno, and I. Terasaki: Phys. Rev. B **70** (2004) 092503.
 - 53) D. J. Scalapino, E. Loh Jr., and J. E. Hirsch: Phys. Rev. B **34** (1986) 8190; N. E. Bickers, D. J. Scalapino, and R. T. Scalettar: Int. J. Mod. Phys. B **1** (1987) 687; H. Shimahara and S. Takada: J. Phys. Soc. Jpn. **57** (1988) 1044.
 - 54) N. E. Bickers, D. J. Scalapino, and S. R. White: Phys. Rev. Lett. **62** (1989) 961.
 - 55) T. Nomura and K. Yamada: J. Phys. Soc. Jpn. **72** (2003) 2053.
 - 56) R. Hlubina: Phys. Rev. B **59** (1999) 9600; J. Kondo: J. Phys. Soc. Jpn. **70** (2001) 808.
 - 57) E. Dagotto, J. Riera, Y. C. Chen, A. Moreo, A. Nazarenko, F. Alcaraz, and F. Ortolani: Phys. Rev. B **49** (1994) 3548.
 - 58) S. Sorella, G. B. Martins, F. Becca, C. Gazza, L. Capriotti, A. Parola, and E. Dagotto: Phys. Rev. Lett. **88** (2002) 117002.
 - 59) T. Giamarchi and C. Lhuillier: Phys. Rev. B **43** (1991) 12943.
 - 60) K. Yamaji, T. Yanagisawa, T. Nakanishi, and S. Koike: Physica C **304** (1998) 225.
 - 61) T. Yanagisawa, S. Koike, and K. Yamaji: J. Phys. Soc. Jpn. **68** (1999) 3608; D. Baeriswyl, D. Eichenberger, and M. Menteshshavilli: New J. Phys. **11** (2009) 075010.
 - 62) T. A. Maier, M. Jarrell, T. C. Schulthess, P. R. C. Kent, and

- 63) D. Sénéchal, P.-L. Lavertu, M.-A. Marois, and A.-M. S. Tremblay: Phys. Rev. Lett. **94** (2005) 156404.
- 64) M. Aichhorn, E. Arrigoni, M. Potthoff, and W. Hanke: Phys. Rev. B **74** (2006) 024508.
- 65) M. Capone and G. Kotliar: Phys. Rev. B **74** (2006) 054513.
- 66) T. K. Lee and S. Feng: Phys. Rev. B **38** (1988) 11809.
- 67) A. Himeda and M. Ogata: Phys. Rev. B **60** (1999) R9935.
- 68) M. Aichhorn, E. Arrigoni, M. Potthoff, and W. Hanke: Phys. Rev. B **74** (2006) 024508; S. S. Kancharla, B. Kyung, D. Sénéchal, M. Civelli, M. Capone, G. Kotliar, and A.-M. S. Tremblay: Phys. Rev. B **77** (2008) 184516.
- 69) T. K. Lee, C.-M. Ho, and N. Nagaosa: Phys. Rev. Lett. **90** (2003) 067001.
- 70) K. Kobayashi and H. Yokoyama: Physica C **469** (2009) 974.
- 71) For instance, A. Hosseini, D. M. Broun, D. E. Sheehy, T. P. Davis, M. Franz, W. N. Hardy, R. Liang, and D. A. Bonn: Phys. Rev. Lett. **93** (2004) 107003.
- 72) H. Mukuda, M. Abe, Y. Araki, Y. Kitaoka, K. Tokiwa, T. Watanabe, A. Iyo, H. Kito, and Y. Tanaka: Phys. Rev. Lett. **96** (2006) 087001; H. Mukuda, Y. Yamaguchi, S. Shimizu, Y. Kitaoka, P. Shirage, and A. Iyo: J. Phys. Soc. Jpn. **77** (2008) 124706.
- 73) C.-H. Lee, A. Iyo, K. Kihou, H. Kito, H. Hiraka, K. Ohoyama, and K. Yamada: J. Phys. Soc. Jpn. **77** (2008) 073706; S. Shimizu, S. Tabata, H. Mukuda, Y. Kitaoka, P. M. Shirage, H. Kito, and A. Iyo: J. Phys. Soc. Jpn. **80** (2011) 043706.
- 74) H. Mukuda, S. Shimizu, A. Iyo, and Y. Kitaoka: J. Phys. Soc. Jpn. **81** (2012) 011008.
- 75) M. Fujita, H. Hiraka, M. Matsuda, M. Matsuura, J. M. Tranquada, S. Wakimoto, G. Xu, and K. Yamada: J. Phys. Soc. Jpn. **81** (2012) 011007.
- 76) K. Kobayashi and H. Yokoyama: J. Low Temp. Phys. **117** (1999) 199; A. Himeda and M. Ogata: Phys. Rev. Lett. **88** (2002) 117001.
- 77) R. Jastrow: Phys. Rev. **98** (1955) 1479.
- 78) M. C. Gutzwiller: Phys. Rev. Lett. **10** (1963) 159.
- 79) H. Yokoyama and H. Shiba: J. Phys. Soc. Jpn. **56** (1987) 1490.
- 80) T. A. Kaplan, P. Horsch, and P. Fulde: Phys. Rev. Lett. **49** (1982) 889.
- 81) H. Yokoyama and H. Shiba: J. Phys. Soc. Jpn. **59** (1990) 3669.
- 82) T. Watanabe, H. Yokoyama, Y. Tanaka, and J. Inoue: J. Phys. Soc. Jpn. **75** (2006) 074707.
- 83) H. Yokoyama: Prog. Theor. Phys. **108** (2002) 59.
- 84) S. Tamura and H. Yokoyama: J. Phys. Soc. Jpn. **81** (2012) 064718, and Phys. Proc. **27** (2012) 76.
- 85) In ref. 17, we displayed the data of μ' at half filling as being twice as large as the correct values in error. The ranges of ordinates in Figs. 4(d) and 15(c) in ref. 17 should be $[-0.05, 0.05]$ and $[0, 0.15]$, respectively. This does not affect the interpretation of the physics.
- 86) J. P. Bouchaud, A. Georges, and C. Lhuillier: J. Phys. (Paris) **49** (1988) 553.
- 87) Although we have checked the optimized energies for the homogeneous and extended s waves, they are never stabilized near half filling. To consider the gap form more precisely, it becomes necessary to include SC correlations with longer Cooper pairs.⁸⁸ According to ref. 88, the optimized gap form somewhat deviates from the simple $d_{x^2-y^2}$ wave, eq. (11). In electron-doped cases, $\Delta_{\mathbf{k}}$ exhibits nonmonotonic behavior,⁸⁹ consistent with the results of experiments.⁹⁰ In hole-doped cases, $\Delta_{\mathbf{k}}$ becomes concave near the node directions, which qualitatively accords with the results of experiments on Bi2212.⁹¹
- 88) T. Watanabe, H. Yokoyama, K. Shigeta, and M. Ogata: New J. Phys. **11** (2009) 075011.
- 89) H. Yoshimura and D. S. Hirashima: J. Phys. Soc. Jpn. **74** (2005) 712; T. Watanabe, T. Miyata, H. Yokoyama, Y. Tanaka, and J. Inoue: J. Phys. Soc. Jpn. **74** (2005) 1942.
- 90) G. Blumberg, A. Koitzsch, A. Gozar, B. S. Dennis, C. A. Kendziora, P. Fournier, and R. L. Greene: Phys. Rev. Lett. **88** (2002) 107002; H. Matsui, K. Terashima, T. Sato, T. Takahashi, M. Fujita, and K. Yamada: Phys. Rev. Lett. **95** (2005)
- 91) H. Ding, M. R. Norman, J. C. Campuzano, M. Randeria, A. F. Bellman, T. Yokoya, T. Takahashi, T. Mochiku, and K. Kadowaki: Phys. Rev. B **54** (1996) R9678; J. Mesot, M. R. Norman, H. Ding, M. Randeria, J. C. Campuzano, A. Paramekanti, H. M. Fretwell, A. Kaminski, T. Takeuchi, T. Yokoya, T. Sato, T. Takahashi, T. Mochiku, and K. Kadowaki: Phys. Rev. Lett. **83** (1999) 840.
- 92) F. C. Zhang, C. Gros, T. M. Rice, and H. Shiba: Supercond. Sci. Technol. **1** (1988) 36.
- 93) K.-Y. Yang, C. T. Shih, C. P. Chou, S. M. Huang, T. K. Lee, T. Xiang, and F. C. Zhang: Phys. Rev. B **73** (2006) 224513.
- 94) A. Himeda and M. Ogata: Phys. Rev. Lett. **85** (2000) 4345.
- 95) T. Watanabe, H. Yokoyama, Y. Tanaka, and J. Inoue: J. Mag. Mag. Mat. **310** (2007) 648; Y. C. Chen: private communication.
- 96) H. Yokoyama and H. Shiba: J. Phys. Soc. Jpn. **67** (1987) 3582, and J. Phys. Soc. Jpn. **67** (1987) 3570.
- 97) W. H. Press, S. A. Teukolsky, W. T. Vetterling, and B. P. Flannery: *Numerical Recipes in FORTRAN* (Cambridge, New York, 1992) 2nd ed. p. 406.
- 98) G. Zheng, P. L. Kuhns, A. P. Reyes, B. Liang, and C. T. Lin: Phys. Rev. Lett. **94** (2005) 047006.
- 99) D. Fournier, G. Levy, Y. Pennec, J. L. McChesney, A. Bostwick, E. Rotenberg, R. Liang, W. N. Hardy, D. A. Bonn, I. S. Elfimov, and A. Damascelli: Nat. Phys. **6** (2010) 905.
- 100) This function form does not correspond to that of a perturbation study of the BCS function for $U \rightarrow 0$:⁵⁶ $\Delta \propto \exp(-t^2/U^2)$. Such a singular term should exist, but probably is dominant only for extremely small U .
- 101) As mentioned in ref. 16, total energies for $U > U_{co}$ at half filling fit very well with $-\gamma t^2/U$ (γ : const.), which corresponds to the result of the strong-coupling (t/U) expansion.
- 102) Y. Yanase and M. Ogata: J. Phys. Soc. Jpn. **74** (2005) 1534.
- 103) P. F. Maldague: Phys. Rev. B **16** (1977) 2437.
- 104) See also Y. Nagaoka: Phys. Rev. **147** (1966) 392.
- 105) As a recent review, M. Vojta: Adv. Phys. **58** (2009) 699.
- 106) For instance, M. Lugas, L. Spanu, F. Becca, and S. Sorella: Phys. Rev. B **74** (2006) 165122, and references therein.
- 107) C.-C. Chang and S. Zhang: Phys. Rev. B **78** (2008) 165101.
- 108) A. Paramekanti, M. Randeria, and N. Trivedi: Phys. Rev. B **70** (2004) 054504.
- 109) H. Kondo and T. Moriya: J. Phys. Soc. Jpn. **78** (2009) 013704.
- 110) Y. Suzumura, Y. Hasegawa, and H. Fukuyama: J. Phys. Soc. Jpn. **57** (1988) 401.
- 111) For instance, R. P. Feynman: *Statistical Mechanics* (Benjamin, Reading, 1972) Chap. 11.
- 112) J. W. Loram, J. Luo, J. R. Cooper, W. Y. Liang, and J. L. Tallon: J. Phys. Chem. Solids **62** (2001) 59.
- 113) T. Matsuzaki, N. Momono, M. Oda, and M. Ido: J. Phys. Soc. Jpn. **73** (2004) 2232.
- 114) L. F. Tocchio, F. Becca, and C. Gros: Phys. Rev. B **83** (2011) 195138.
- 115) In a strict sense, the hopping of a holon (or doublon) of a D-H pair is counted in E_h if the holon is separated by more than one lattice spacing from the partner doublon (in a process higher than the second order). However, such a process occurs very rarely for large values of U/t , and thus may be neglected.²⁰ Incidentally, the contribution of three-site (pair-hopping) terms, if we take them into account, is included in E_d .
- 116) It was shown by S. Tamura that the Drude weight is broadly proportional to E_h for $U > U_c$ (private communication).
- 117) H. Takagi, B. Batlogg, H. L. Kao, J. Kwo, R. J. Cava, J. J. Krajewski, and W. F. Peck, Jr.: Phys. Rev. Lett. **69** (1992) 2975; S. Uchida, T. Ido, H. Takagi, T. Arima, Y. Tokura, and S. Tajima: Phys. Rev. B **43** (1991) 7942; N. Momono, M. Ido, T. Nakano, M. Oda, Y. Okajima, and K. Yamaya: Physica C **233** (1994) 395; T. Yoshida, X. J. Zhou, K. Tanaka, W. L. Yang, Z. Hussain, Z.-X. Shen, A. Fujimori, S. Sahrakorpi, M. Lindroos, R. S. Markiewicz, A. Bansil, S. Komiya, Y. Ando, H. Eisaki, T. Kakeshita, and S. Uchida: Phys. Rev. B **74** (2006) 224510.

- W. D. Wu, J. H. Brewer, T. M. Riseman, C. L. Seaman, M. B. Maple, M. Ishikawa, D. G. Hinks, J. D. Jorgensen, G. Saito, and H. Yamochi: Phys. Rev. Lett. **66** (1991) 2665.
- 119) G. Xu, G. D. Gu, M. Hücker, B. Fauqué, T. G. Perring, L. P. Regnault, and J. M. Tranquada: Nat. Phys. **5** (2009) 642.
- 120) T. Watanabe, H. Yokoyama, Y. Tanaka, J. Inoue, M. Ogata: J. Phys. Chem. Solids **67** (2006) 112.
- 121) M. Matsuda, M. Fujita, K. Yamada, R. J. Birgeneau, Y. Endoh, and G. Shirane: Phys. Rev. B **65** (2002) 134515.
- 122) M. Fujita, T. Kubo, S. Kuroshima, T. Uefuji, K. Kawashima, K. Yamada, I. Watanabe, and K. Nagamine: Phys. Rev. B **67** (2003) 014514.
- 123) T. Watanabe, H. Yokoyama, Y. Tanaka, and J. Inoue: Phys. Rev. B **77** (2008) 214505.
- 124) K. Kobayashi and H. Yokoyama: Physica C **463-465** (2007) 141, and J. Phys. Chem. Solids **69** (2008) 3274.
- 125) Actually, it is not easy to optimize cases of $t'/t = -0.4$, $n = 0.80$, $L = 10$, and $10 \lesssim U/t \lesssim 20$, because the variational energies become almost the same for $0.05 \lesssim \Delta_d/t \lesssim 0.16$, which yields $0.002 \lesssim P_d^\infty \lesssim 0.015$, suggesting that this parameter set is situated near the transition point. We refrain from using the data of this parameter set in the figures.
- 126) L. F. Tocchio, F. Becca, and C. Gros: Phys. Rev. B **86** (2012) 035102.
- 127) For instance, D. J. Scalapino, E. Loh Jr., and J. E. Hirsch: Phys. Rev. B **34** (1986) 8190; K. Miyake, S. Schmitt-Rink, and C. M. Varma: Phys. Rev. B **34** (1986) 6554.
- 128) S. R. White and D. J. Scalapino: Phys. Rev. B **60** (1999) R753.
- 129) G. B. Martins, J. C. Xavier, L. Arrachea, and E. Dagotto: Phys. Rev. B **64** (2001) 180513.
- 130) Although we use a bare band here, it is more appropriate to consider a renormalized band owing to the effect of U , which is a future problem.
- 131) $n(\mathbf{k})$ seems stationary at $(\pi, 0)$ at half filling by inferring from the system-size dependence of $|\nabla n(\mathbf{X}')|$ [see L in Fig. 31(e)]. For $\delta \lesssim 0.05$, owing to regular and strong system-size dependence, the behavior of $|\nabla n(\mathbf{X}')|$ for $L = \infty$ is likely to resemble that of P_d^∞ .
- 132) M. Aichhorn, E. Arrigoni, Z. B. Huang, and W. Hanke: Phys. Rev. Lett. **99** (2007) 257002.
- 133) M. Civelli, M. Capone, A. Georges, K. Haule, O. Parcollet, T. D. Stanescu, and G. Kotliar: Phys. Rev. Lett. **100** (2008) 046402.
- 134) S. Sorella: Phys. Rev. B **64** (2001) 024512; C. J. Umrigar and C. Filippi: Phys. Rev. Lett. **94** (2005) 150201.
- 135) D. Tahara and M. Imada: J. Phys. Soc. Jpn. **77** (2008) 093703, and J. Phys. Soc. Jpn. **77** (2008) 114701.
- 136) P. Phillips: Rev. Mod. Phys. **82** (2010) 1719; Y. Yamaji and M. Imada: Phys. Rev. B **83** (2011) 205122.
- 137) A. B. Harris and R. V. Lange: Phys. Rev. **157** (1967) 295; J. E. Hirsch: Phys. Rev. Lett. **54** (1985) 1317.
- 138) P. Fazekas, Phys. Scr. **T29** (1989) 125.
- 139) In Table B·1, the energy of Q_j^S is unexpectedly close to that of an improved asymmetrized factor Q_j^{DH} even for $n = 0.8$. If we disregard the argument of D-H symmetry, Q_j^S may be used for $n < 1$. In this connection, we erroneously described in ref. 16 that Q_j^S does not work for $n \neq 0$ and $U > 0$.
- 140) We adopt the stepwise or Manhattan metric to measure $|\mathbf{r}|$.